Security of position-based quantum cryptography limits Hamiltonian simulation via holography

Harriet Apel^a, Toby Cubitt^a, Patrick Hayden^b Tamara Kohler^c, David Pérez-García^c

^aDepartment of Computer Science, University College London, UK ^bStandford Institute for Theoretical Physics, Stanford University ^cInstituto de Ciencias Matemáticas, Madrid

Abstract

We investigate the link between position-based quantum cryptography (PBQC) and holography established in [MPS19] using holographic quantum error correcting codes as toy models. If the "temporal" scaling of the AdS metric is inserted by hand into the toy model via the bulk Hamiltonian interaction strength we recover a toy model with consistent causality structure. This leads to an interesting implication between two topics in quantum information: if position-based cryptography is secure against attacks with small entanglement then there are new fundamental lower bounds for resources required for one Hamiltonian to simulate another.

Contents

1	Introduction	1
2	2.3 Sending a particle through the bulk/around the boundary	
3	Secure finite dimensional PBQC implies an upper bound on simulation techniques 3.1 Position-based quantum cryptography	8 8 9 11 17
4	Discussion 4.1 Toy models of AdS/CFT	18 18 18
Aı	Appendices	
A	Motivation of matching lower bound for boundary entanglement	19
В	An explicit non-perturbative construction of an attack on PBQC	20
\mathbf{C}	Explicit perturbative construction of an attack on PBQC	24
D	Lower bound on simulation from causality	28

1 Introduction

Anti-de Sitter spacetime is described by the metric:

$$ds^{2} = \alpha^{2} \left(-\cosh^{2} \rho dt^{2} + d\rho^{2} + \sinh^{2} \rho d\Omega_{d-2}^{2} \right), \tag{1}$$

where in the limit $\rho \to \infty$ we approach the boundary of the spacetime. Holographic tensor networks models of the AdS/CFT correspondence [Pas+15; Hay+16; KC19; Koh+20; AKC21] encode the "spatial" component of the AdS metric by placing the tensors in the cells of a honeycombing of hyperbolic space. These models capture various features of AdS/CFT while being exactly solvable. The bulk theory acts on a free index of each tensor while the boundary theory acts on the dangling indices at the truncation of the tessellation. This truncation occurs at a fixed radius, R, that can be taken to be arbitrarily large and is what allows these models to be finite dimensional.

These models provide an encoding map from bulk to boundary and vice versa, realising various aspects of the correspondence explicitly: complementary recovery, Ryu-Takayanagi and a duality between local models. One could hope to explore dynamics in a semi-classical geometry by considering the dual bulk/boundary Hamiltonians associated with the toy models on space-like slices. However, the proposed dictionaries lead to superluminal signalling on the boundary. In [Pas+15; Hay+16] the boundary operations are non-local, allowing for instantaneous interactions between separate boundary regions. In [AKC21; KC19; Koh+20] this is improved to give a bulk-boundary mapping that maps (quasi)-local Hamiltonians in the bulk to local Hamiltonians on the boundary. Even so, the local boundary operations have large interaction strengths which still leads to unbounded signalling speeds on the boundary. However, from the AdS metric it is manifest that coordinate time is not spatially uniform, but instead exponentially dilates as the observer falls into the bulk. We argue that to obtain a toy model with consistent causal structure this "time" component of the metric needs to be fixed by hand.

By selecting a bulk Hamiltonian that incorporates this time dilation, we can demonstrate that the resulting tensor network model of holography exhibits the anticipated causal structure, satisfying:

- 1. The time taken for a particle travelling across the bulk is consistent with the dual particle travelling around the boundary (Fig. 1).
- 2. The bulk to boundary recovery map gives dual operators that are smeared out (non-local) on the boundary but *in straight light cones* giving constant butterfly velocities ¹ (Fig. 1).

Both of these features of consistent causality were missing in previous toy models of holography where there was no constraint on the bulk Hamiltonian.

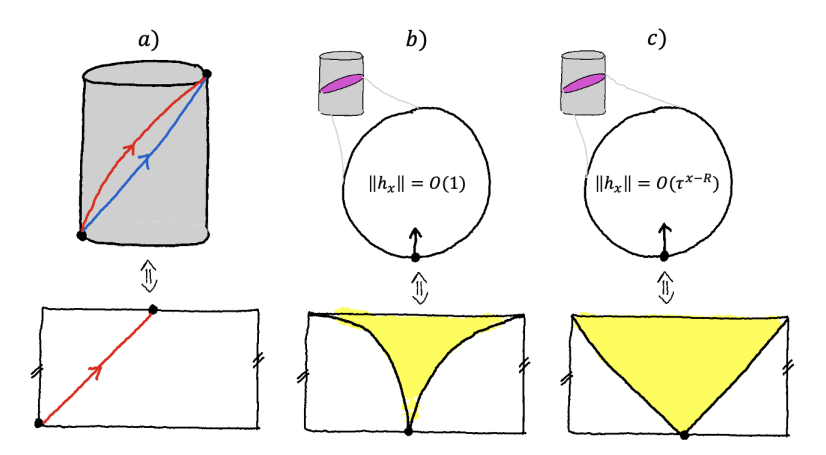


Figure 1: a) With the bulk Hamiltonian norm scaling as in Eq. (14), the time taken for a particle to travel through the finite bulk is consistent with the time taken for the particle to travel around the boundary in the dual theory. b) Ignoring the time dilation of the metric creates boundary butterfly velocities are not constant so that as a bulk object propagates to the center of the bulk the speed at which information on the boundary spreads increase. This leads to non-linear causal cones on the boundary. c) Accounting for time dilation recovers linear causal cones for recovered boundary operations.

One motivation behind constructing tensor network toy models of AdS/CFT with the correct causality structure is to investigate position-based cryptography (PBQC) within these models. It has been argued that if arbitrary computations can occur in the bulk of AdS, then the bulk-boundary

¹Butterfly velocities give an effective maximum speed of propagation of any operator but restricted to – in this case – the code subspace of low energy excitation on a classical background geometry that cause negligible back reaction as in [QY17].

correspondence indicates that PBQC can be broken using only linear entanglement [MPS19; May19; DC22a]. This is exponentially better than the best known quantum information protocols [Buh+14; BK11b; CM22; DC22b], and there is evidence that such protocols cannot exist [Jun+22]. The mismatch between quantum information and holography has led to speculation that gravity may constrain computation in some way [May22].

In this work we study position-based cryptography protocols in tensor network toy models of AdS/CFT that have the improved causality structure. While the construction does not provide a holography-inspired PBQC protocol that beats the best known quantum information protocols, it does allow us to relate two seemingly distinct fields of study in quantum information: PBQC and Hamiltonian simulation. Hamiltonian simulation refers to the task of reproducing aspects of a target Hamiltonian up to some controllable error using qualitatively different interactions e.g. with respect to locality, geometrical structure, interaction type or symmetries. We are able to show that if PBQC is secure against attacks with linear entanglement then this implies fundamental limits on Hamiltonian simulation techniques that recreate the time dynamics of target Hamiltonians:

Theorem 14 (PBQC and simulation (informal)). If position-based quantum cryptography is secure against attacks with linear entanglement, then for any universal family of 2-local Hamiltonians M^2 there exists some target Hamiltonian $H_{\rm target}$ acting on N spins such that the local interaction strength required to simulate $H_{\rm target}$ with a Hamiltonian from M is lower bounded by a polynomial in the ratio of N to the desired error in the simulation.

See the formal statement of Theorem 14 along with Definition 3 and Definition 8, for a rigorous statement of the result, which outlines the lower bounds in more detail.

It has previously been shown in [AZ18] that there exist 2-local, all-to-all interactions which cannot be simulated by 2-local interactions with constant degree using O(1) interaction strength. If the security of PBQC against attacks with linear entanglement was demonstrated then Theorem 14 would give new lower bounds on achievable simulations. Note that in our result by linear entanglement we mean that the mutual information shared between non-local parities is upper bounded by C_1n where we have $C_1 > 1$. N, the number of qubits supporting H_{target} in Theorem 14 is proportional to n, the number of qubits on which the local unitary in the position based protocol acts on. Since the constant C_1 is greater than 1, it is not known whether PBQC is secure against attacks of this type as we are outside the regime in [Tom+13] where it is known to be insecure³.

There are currently no known Hamiltonian simulation methods that achieve the interaction strength scaling in Theorem 14. Our argument implies that the existence of such techniques would provide a protocol to break position-based cryptography with only linear entanglement. Note that the converse is not true – it may be possible to break position-based cryptography via other methods that say nothing about fundamental limits of simulation.

While Theorem 14 is stated in terms of general unitaries and general Hamiltonians, there is an immediate corollary about the security of families of unitaries and the complexity of simulating the corresponding Hamiltonians. The corollary says that the Hamiltonians that correspond to unitaries that are secure for PBQC are hard to simulate.⁴ Imposing no structure on the bulk unitary, and using Theorem 14 to bound the resources required to simulate global Hamiltonians, gives a no-go result that is in line with what could be expected from physical intuition. However, when considering restricted classes of unitaries the bound implied by holography becomes tighter. For example, non-trivial unitaries for PBQC can be generated by k-local bulk Hamiltonians which leads to H_{target} being sparse. In this case by optimising existing simulation techniques we can in fact come very close to saturating the bound from Theorem 14. If the bound could be saturated it would imply that unitaries generated by k-local bulk Hamiltonians cannot be used in PBQC protocols that are secure against linear entanglement. While if it is shown that such unitaries can provide secure PBQC protocols, it would imply that the simulation technique derived here is close to optimal for this class of Hamiltonians. Previous results have shown that circuits that have low complexity as measured by their T-gate count [Spe16] do not provide secure unitaries for PBQC.⁵ Our result can be viewed as another way of exploring this relationship between security for PBQC and complexity.

²We say that a family \mathcal{M} of Hamiltonians is universal if for any target Hamiltonian H_{target} there exists an $H \in \mathcal{M}$ that can simulate H_{target} .

³It is known that protocols exist that are secure against adversaries with at most C_1n entanglement where $C_1 < -\log_2\left(\frac{1}{2} + \frac{1}{2\sqrt{2}}\right)$ [Tom+13].

⁴Note that the hard-to-simulate Hamiltonian that corresponds to the unitary is not quite the Hamiltonian that generates the unitary – it is related to this Hamiltonian by an isometric mapping – see Corollary 15 for details.

⁵In [Spe16] it is demonstrated PBQC protocols using circuits with logarithmic numbers of T gates can be broken using only polynomial entanglement.

In the first section of this paper we describe how the time dilation described above can be fixed by hand into the tensor network models to yield the features of consistent causal structure described above, Section 2. In the second half we then use these models to prove Theorem 14 in Section 3.3 for a strong definition of simulation where we have a relationship between simulation parameters. We then compare the bounds on simulation in Theorem 14 to the optimised version of best-known simulation techniques for sparse Hamiltonians.

2 Causal structure of toy models of AdS/CFT from time dilation

2.1 Time dilation in the bulk

The bulk is described by the AdS metric. In this metric time for an observer in the centre of the bulk is dilated with respect to the time experienced by an observer sitting on the conformal boundary. This can be seen by looking at the AdS_d metric in global coordinates

$$ds^{2} = \alpha^{2} \left(-\cosh^{2} \rho dt^{2} + d\rho^{2} + \sinh^{2} \rho d\Omega_{d-2}^{2} \right)$$

$$\tag{2}$$

where $\rho \in \mathbb{R}^+$ and in the limit $\rho \to \infty$ we approach the boundary of the spacetime. α is the radius of curvature, related to the cosmological constant by $\Lambda = \frac{-(d-1)(d-2)}{2\alpha^2}$. At fixed "spatial" position $(\rho, \mathbf{\Omega})$ the proper time $d\mathcal{T} = -ds$ is given by,

$$d\mathcal{T} = \alpha \cosh \rho dt. \tag{3}$$

This "time dilation" can be observed by comparing the coordinate time for two observers at different distances into the bulk. Consider one observer at ρ_0 and one at ρ_1 with $0 < \rho_0 < \rho_1$. The relationship between the two coordinate times with the same proper time is,

$$dt_0 = \frac{\cosh \rho_1}{\cosh \rho_0} dt_1. \tag{4}$$

Note that $dt_0 > dt_1$ since for positive arguments cosh is monotonically increasing $\frac{\cosh \rho_1}{\cosh \rho_0} > 1$.

2.2 "Fixing" time dilation in the toy model

The "spatial" component of the AdS metric is incorporated into the model by placing the tensors in the cells of a honeycombing of hyperbolic space. In order to emulate the "time" component of the metric we need to insert this dilation by hand. Since this is a finite model we consider a truncated version of AdS space time where instead of infinity the conformal boundary exists at a fixed maximum radius, R, that can be taken to be arbitrarily large. This truncation fixes a "central" tensor that represents the deepest part of the bulk. In translating the metric onto the tensor network model the distance from the centre of the bulk is now quantified by the number of layers of tensors from this central tensor, which we denote $x \in \mathbb{Z}^+$ (see Fig. 2).

In constructing a tensor network toy model there are a number of free parameters: the radius of truncation R, the local Hilbert space dimension d_b of each dangling leg associated with the bulk degrees of freedom and the local Hilbert space dimension d_{∂} of the tensor legs contracted in the bulk and associated with the boundary degrees of freedom. For convenience in later sections we chose to make each tensor 'leg' a bundle of qubits rather than a singular qudit. We will denote the bulk legs to be n qubits and the legs contracted in the bulk and left dangling at the boundary to be each m qubits, as in Fig. 2. In constructions using perfect tensors n=m, whereas in random tensor constructions it is essential for the desirable features of the models to take $m \gg n$.

There is a choice when relating the natural "radius" in the tensor network model to the measure of radius in the metric, ρ . The relationship between the value of ρ at position x, denoted ρ_x , and x must be consistent with how the curvature of AdS space causes the length swept out by the "angle" coordinate to grow as the radius increases. In the tensor network picture the surface area at x is given by the number of degrees of freedom in that layer N(x). If each tensor has n dangling bulk indices, the length then corresponds to n times the number of tensors in the layer, which grows with x exponentially giving:

$$N(x) \propto n\tau^x$$
, (5)

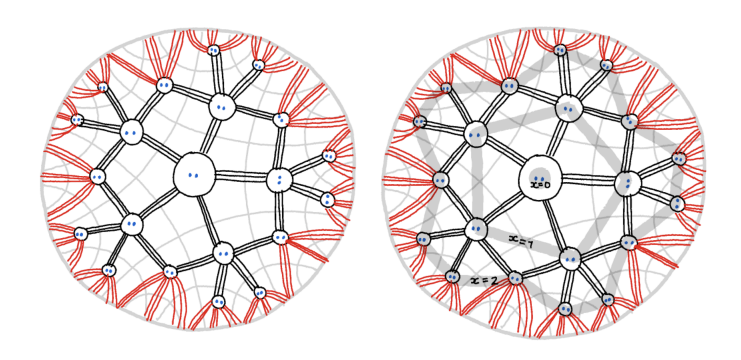


Figure 2: Left) tensor network with n=2 and m=3. Right) Bulk of AdS. x denotes the position from the centre and the conformal boundary is at R=2.

where τ is the growth rate of the Coxeter group associated with the hyperbolic honeycombing. To be consistent N(x) should correspond to the circumference of a circle with radius ρ_x , $c(\rho_x)$, as taken from the metric in Eq. (1):

$$c(\rho_x) = \int_0^{2\pi} \sinh \rho_x d\Omega = 2\pi \sinh \rho \sim e^{\rho}. \tag{6}$$

Equating Eq. (5) and Eq. (6) gives the correspondence between x and ρ_x :

$$N(x) = c(\rho_x) \tag{7}$$

$$n\tau^x = e^{\rho_x} \tag{8}$$

$$x \ln \tau + \ln n = \rho_x. \tag{9}$$

Therefore, the coordinate time at the truncated boundary t_R is related to the coordinate time in the bulk at the x'th tensor layer by,

$$dt_x = \frac{\cosh \rho_R}{\cosh \rho_x} dt_R \tag{10}$$

$$dt_x = \frac{\cosh \rho_R}{\cosh \rho_x} dt_R$$

$$= \frac{e^{\ln(n\tau^R)} + e^{-\ln(n\tau^R)}}{e^{\ln(n\tau^x)} + e^{-\ln(n\tau^x)}} dt_R$$
(10)

$$\sim \tau^{R-x} dt_R. \tag{12}$$

Note the scaling is independent of n and m.

In holography the entire physics of the bulk has a representation on the boundary, hence in order to consider a boundary theory associated with a boundary coordinate time it is more convenient to put in this time dilation into the bulk Hamiltonian as a renormalisation. This is mathematically equivalent since the Hamiltonian and time always appear in a product. Assume we have a geometrically 2-local Hamiltonian in the bulk where interacting terms only occur between tensors in neighbouring tessellation cells:

$$H_{\text{bulk}} = \sum_{i} h_x^{(i)},\tag{13}$$

where h_x acts trivially on all tensors in layers y < x of the tessellation (since the Hamiltonian is 2-local it will also act trivially on the majority of tensors in layers $\geq x$ but for time dilation this is less relevant).

To encode the time dilation scaling in Eq. (12) the norm of the bulk interaction terms should decay exponentially towards the centre of the bulk:

$$||h_x|| = O\left(\tau^{x-R}\right). \tag{14}$$

Therefore the Hamiltonian terms acting at x = R are O(1) which is consistent since only here do the "bulk" and "boundary" proper time immediately coincide.

Sending a particle through the bulk/around the boundary 2.3

We have argued that choosing a bulk Hamiltonian that scales as Eq. (14) is necessary to have causal structure in the bulk/boundary in a toy model of holography consistent with the AdS metric.⁶ It

⁶As a sanity check this exponential scaling is seen in the Hamiltonian of a free particle moving in AdS: $H_{\text{free particle}} = \int d\rho d\phi \cosh \rho \left(\tanh \rho d\psi_0\right)^2$

is notable that a similar exponential envelope on the interaction strengths is also exactly what is used in [BS23] to obtain the correct specific heat capacity of the SYK model from a MERA-like network. Consistent causal structure is manifest when we consider a particle travelling from one side of the boundary to the other as in Fig. 3.

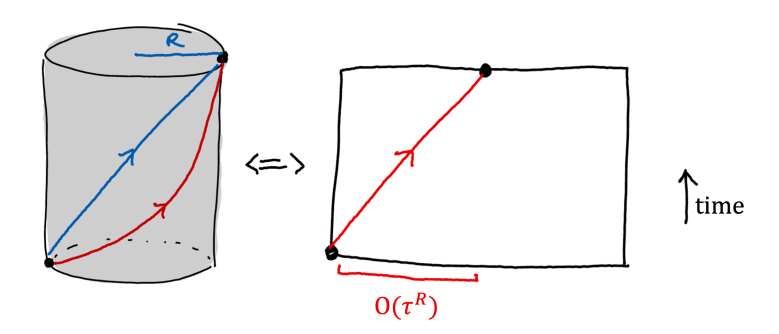


Figure 3: Sending a particle sent through the bulk/around the boundary.

In the bulk theory the particle falls in to the bulk from the asymptotic boundary and eventually reaches the other asymptotic boundary evolving under the bulk Hamiltonian. In the boundary theory the particle travels around the boundary. If the bulk and boundary Hamiltonian had uniform norm the particle only has to make O(R) 'tensor jumps' to cross the bulk but $O(\tau^R)$ 'tensor jumps' to cross the boundary. Therefore, clearly the two theories would take different times to achieve the same outcome – moving the particle across the boundary – breaking the consistency of the holographic picture.

Under a Hamiltonian with interaction scaling as Eq. (14), it takes the falling particle $O(n\tau^{R-x})$ time to travel from tensor layer x+1 to x, an O(n) distance. Hence the particle takes time

$$T_1 = 2n \sum_{x=0}^{R} \tau^{R-x} = \frac{2n(\tau^{R+1} - 1)}{\tau - 1} = O(n\tau^R), \tag{15}$$

to travel through the bulk. Assuming a geometrically 2-local boundary Hamiltonian with all interactions scaling as $||h_R|| = O(1)$ to be consistent with Eq. (14), the particle takes time

$$T_2 = \sum_{i=0}^{O(m\tau^R)} 1 = O(m\tau^R), \tag{16}$$

to travel around the boundary.

The scalings of T_1 and T_2 match up with respect to R, hence by choosing an appropriate bulk Hamiltonian we have restored a consistent causal structure for this basic task. If $m \neq n$ then the boundary Hamiltonian must scale as the ratio $||h_{\text{boundary}}|| = O(m/n)$ to recover $T_1 = T_2$. It is important that the exponential decay of the bulk Hamiltonian norm have the exponent given in Eq. (14). Having even a different constant factor in the exponent would cause the above bulk/boundary tasks to take different times and therefore lose the connection to holography.

2.4 Causal behaviour of perturbations from butterfly velocities

Another motivation for rescaling the bulk Hamiltonian is that when considering a bulk perturbation, the dual boundary causal cone is now straight, with constant velocity regardless of where the perturbation is in the bulk. In previous models with uniform strength bulk Hamiltonians the information would appear to propagate faster on the boundary, the deeper the dual excitation is in bulk. The rescaling makes sense of this peculiarity and we will use argument for straight boundary light cones in the construction of the PBQC protocol later.

We will consider use the bulk Lieb-Robinson velocity to determine the butterfly velocity via the duality. In the bulk there is a geometrically 2-local Hamiltonian that respects the metric of the bulk. The Lieb-Robinson velocity is the maximum speed that information can propagate in a theory, formally, **Definition 1** (Lieb-Robinson velocity). Given a k-local Hamiltonian, $H = \sum_{Z} h_{Z}$ such that $\exists \mu, s > 0$ where for all qudits $i: \sum_{Z \ni i} \|h_{Z}\| \leq se^{-\mu}$. If A_{X} and B_{Y} are operators actin on subsets of qudits X, Y then,

$$||[A_X(t), B_Y]|| \le \min\{|X|, |Y|\} ||A|| ||B|| e^{-\mu(d(X,Y) - vt)},$$
(17)

where d(X,Y) is the interaction distance between sets X and Y and $v = \frac{2ks}{\mu}$ is the Lieb-Robinson velocity.

While Lieb-Robinson speeds bound the propagation of any operator, butterfly velocities give an effective maximum speed of propagation of any operator restricted to a given subspace of the Hilbert space. In [QY17] they study butterfly velocities in the context of holography where the subspace in question is the code subspace of low energy excitation on a classical background geometry that cause negligible back reaction. In the tensor network picture, these holographic butterfly velocities correspond to restricting the boundary to the codespace associated with a fixed tensor geometry with a tensor present in each cell of the tessellation. Formally,

Definition 2 (Butterfly velocity $v(O_A, \mathcal{H}_c)$; [QY17]). Given a boundary code subspace, \mathcal{H}_c and a boundary operator supported on boundary region A, O_A . The butterfly velocity, $v(O_A, \mathcal{H}_c)$ is the minimum velocity such that $\forall \epsilon > 0 \; \exists \; \delta > 0$ where $\Delta t < \delta$ and the following two statements are satisfied:

1. If
$$D > (v(O_A, \mathcal{H}_c) + \epsilon) \Delta t$$
 then
$$\forall B \in \{R | d(R, A) = D\}$$

$$\forall O_B \text{ supported in boundary region } B$$

$$\forall |\psi_i\rangle, |\psi_j\rangle \in \mathcal{H}_c:$$

$$\langle \psi_i | [O_A, O_B] | \psi_j\rangle = 0.$$
2. If $D < (v(O_A, \mathcal{H}_c) - \epsilon) \Delta t$ then
$$\exists C \in \{R | d(R, A) = D\}$$

$$\exists O_C \text{ supported in boundary region } C$$
(18)

Where d(A,B) is the minimum distance (measured by the number of hops in the Hamiltonian interaction graph) between two points $x \in A$ and $y \in B$.

 $\langle \psi_i | [O_A, O_C] | \psi_i \rangle \neq 0.$

 $\exists |\psi_i\rangle, |\psi_j\rangle \in \mathcal{H}_c$:

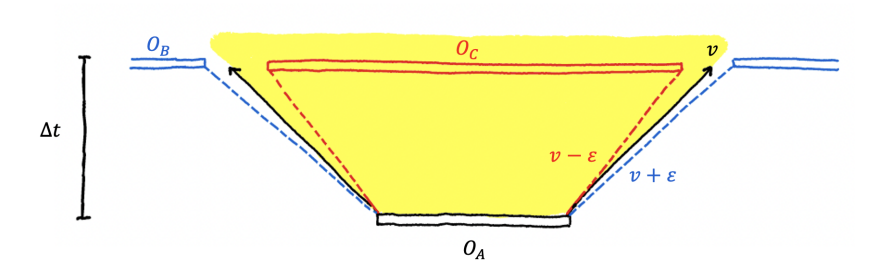


Figure 4: Depiction of the definition of butterfly velocity given in Definition 2.

Section 4 of [QY17] describes how a bulk theory with a known speed of light determines the boundary butterfly velocity. See Fig. 5 for a summary.

The complementary recovery feature necessary for the butterfly velocity argument in [QY17] is exhibited in many tensor network models of AdS/CFT, for example [Pas+15; Hay+16; KC19; Koh+20; AKC21]⁸. For a geometrically 2-local bulk Hamiltonian with individual interactions bounded in norm by Eq. (14) a bulk Lieb-Robinson velocity is given by

$$v_{\text{bulk}}(x) = 2||h_x|| = O(\tau^{x-R}).$$
 (20)

(19)

 $^{^{7}}$ See [KC19] section 3.2 for a discussion of how considering a superposition of multiple networks with different tensors removed could encode dynamical geometry.

⁸For the networks comprised of perfect tensors there are some pathogenic boundary subregions where complementary recovery is violated, however it was shown in [AKC21] with a network of random stabilizer tensors and special tessellations that this holds for any boundary subregion.

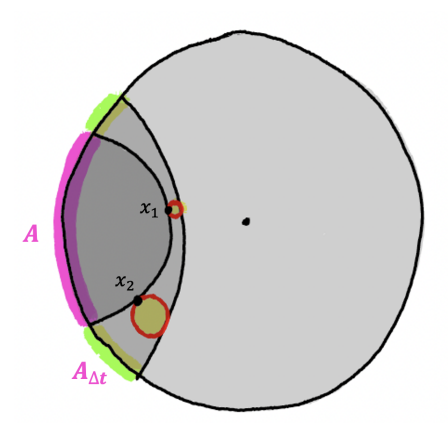


Figure 5: Bulk Lieb-Robinson speed gives boundary butterfly velocity. In AdS/CFT a boundary subregion A can recover any bulk operator that lies within its entanglement wedge, defined by the extremal surface γ_A homologous to A. The same subregion A contains no information about bulk operators outside of this entanglement wedge. At boundary time t=0 consider a boundary subregion A and its extremal surface γ_A . Take any bulk point x infinitesimally inside the entanglement wedge from γ_A . Any bulk operator supported at x, ϕ_x , can be reconstructed on the boundary subregion A, $O_A[\phi_x]$. The butterfly velocity $v(O_A[\phi_x], \mathcal{H}_c)$ for the codespace \mathcal{H}_c is equal to the minimal velocity v^* such that the extremal surface bounding the expanded region $\{A_{\Delta t}|d(A,A_{\Delta t})=v^*\Delta t)\}$ is tangential to the light-cone of x in the bulk defined by the bulk Lieb-Robinson velocity. This figure depicts that if the bulk operator is picked at a smaller radius x_1 along the minimal geodesic than another x_2 , then this formalism implies that the light cone spread at x_1 must be smaller than at x_2 in order to coincide with the minimal geodesic of $A_{\Delta t}$.

Hence the bulk Lieb-Robinson velocity varies with the depth into the bulk – a feature of inserting by hand the dilation of proper time.

Consider a connected subregion of the boundary, A_t where the deepest the entanglement wedge extends into the bulk is to layer x+1. Complementary recovery and the geometry of the tessellation dictates the subregion will contain $O(m\tau^{R-x-1})$ boundary qubits. By the same argument the augmented boundary subregion $A_{t+\Delta t}$ that now extends deeper into the bulk to the x'th layer contains $O(m\tau^{R-x})$ boundary qubits. By butterfly velocities, the causal boundary subregion has increased by $(\tau-1)m\tau^{R-x-1}=O(m\tau^{R-x})$ boundary qubits while the bulk particle has moved from layer x+1 to layer x. Now consider the lightcone of the edge of the entanglement wedge of A_t . By choosing a bulk Hamiltonian to scale as in Eq. (14) the boundary-coordinate-time for the lightray to reach the x'th layer from the (x+1)'th layer is $O(n\tau^{R-x})$. Therefore the boundary butterfly velocity is O(m/n) crucially independent of R and x.

Therefore via butterfly velocities this section has argued that given any holographic tensor network model that exhibits complementary recovery, if a local Hamiltonian with exponentially decaying interaction strength is placed in the bulk, then local bulk operators are smeared out non locally in the boundary in straight light cones. This implies a local boundary Hamiltonian that also has a fixed speed of light as expected in CFTs. Restricting the bulk Hamiltonian to those that reflect the time dilation of the AdS metric is necessary for this aspect of the causal structure of the correspondence to be observed in toy models.

3 Secure finite dimensional PBQC implies an upper bound on simulation techniques

3.1 Position-based quantum cryptography

A key motivation for exploring the causal structure of holographic toy models is the potential of holographic protocols to provide insight into the security of position-based quantum cryptography (PBQC).

The fundamental idea behind PBQC is that the physical location of a party serves as a unique identifier and can be used to establish trust. Unlike traditional cryptographic schemes that rely on keys and passwords, the authentication factor here is position in space-time. A group of adversaries outside of the specified region would compromise the security of the PBQC protocol if they could

spoof the verifiers into believing they are in the prescribed location. It is known that it if the adversaries are allowed to share arbitrary entangled states then they can break any PBQC protocol [Buh+14]. However, sharing arbitrary entangled states is a strong requirement in practise. The key question for determining security of PBQC is: how much entanglement do the attackers have to share to spoof the secure location? Given that the honest prover implements some local operation on n qubits, it is known that the upper bound on the minimal amount of entanglement required is $O(\exp(n))$ [BK11a; Dol]. This would indicate that the protocol is reasonably secure. However, the known lower bounds are only O(n), [Tom+13]. Therefore tightening the bounds on the optimal entanglement required to spoof PBQC is an interesting open question.

Definition 3 (Upper bounded linear attacks). An upper bounded linear attack on a PBQC protocol is any attack where the pre-shared state held by the adversaries has mutual information upper bounded by C_1n for some constant $C_1 > 1$, where n is the number of qubits the unitary acts on in an honest implementation of the protocol.

A protocol is secure against upper bounded linear attacks then there is no attack for all constants C_1 that can break the security.

3.1.1 Connection between PBQC and holography

[May19] introduced the concept of asymptotic quantum tasks, where a quantum information processing task is carried out in the bulk of AdS with inputs given and received at the conformal boundary of the spacetime. In this context the holographic principle states that asymptotic quantum tasks are possible in the boundary if and only if they are possible in the bulk. Given AdS/CFT in (2+1)-dimensional bulk, it is possible to place the inputs and outputs of the task such that in the bulk there exists a causal region included in all four lightcones of the delivery/receiving points such that the boundary corresponding causal region is empty (see Fig. 10). In the bulk, the task can be trivially completed: the inputs can be brought together and a local unitary applied before sending the outputs the delivery points. However, while the holographic principle states that this implies the same task must be feasible on the boundary, there is no local region on the boundary where the computation can take place. The boundary task must be completed via a non-local protocol where local operators act outside the totally connected causal region such that together with communication and entanglement the task is achieved.

[May19] and [MPS19] suggested that such a holography scattering experiment could be a interesting candidate for an attack on PBQC with low entanglement.

3.2 Hamiltonian simulation

The next section will prove the main result of this paper – a link between Hamiltonian simulation and position-based quantum cryptography. Before delving into that result, we will first introduce the basics of Hamiltonian simulation. In Hamiltonian simulation the goal is to engineer a simulator Hamiltonian $H_{\rm sim}$ to reproduce some aspect of a target Hamiltonian $H_{\rm target}$ up to a controllable error. There are a number of definitions for Hamiltonian simulation in the literature. In order to compare the lower bounds on simulation with the best known simulation techniques we need to pick a particular definition of simulation. Here we choose to study the definition from [CMP19], as this is the definition of simulation where errors are best understood.

Any simulation of H_{target} by H_{sim} must involve encoding H_{target} in H_{sim} in some way. In [CMP19] it was shown that any encoding map $\mathcal{E}(\cdot)$ which satisfies basic requirements to be a good simulation must be of the form:

$$\mathcal{E}(A) = V\left(A \otimes P + \overline{A} \otimes Q\right) V^{\dagger} \tag{21}$$

where V is an isometry, P, Q are orthogonal projectors onto some ancillary systems and the overline denotes complex conjugation.

We will be interested in simulations of spin-lattice models, described by local-Hamiltonians where the target system can be decomposed as $\mathcal{H}_{\text{target}} = \bigotimes_{i=1}^{n} \mathcal{H}_{i}$. We say an encoding is *local* if the simulator system can be decomposed as $\mathcal{H}_{\text{sim}} = \bigotimes_{i=1}^{n} \mathcal{H}'_{i}$ such that \mathcal{H}'_{i} corresponds to \mathcal{H}_{i} operationally.

Definition 4 (k-local Hamiltonian). Given a Hamiltonian $H = \sum_j h_j$ on n qudits $(\mathbb{C}^d)^{\otimes n}$. We say that H is k-local if each h_j acts 'non-trivially' on a subset S_j of at most k qubits and as the identity everywhere else. I.e.

$$\forall j: h_j = h_{S_i} \otimes \mathbb{1}_{n \setminus S_i} \text{ and } |S_j| \leq k.$$

Encodings capture the idea of one Hamiltonian perfectly replicating the physics of another. To allow for some controllable error we introduce the concept of an approximate simulation:

Definition 5 (Approximate simulation [CMP19]). We say that H_{sim} is a (Δ, η, ϵ) -simulation of H_{target} if there exists a local encoding $\mathcal{E}(M) = V\left(M \otimes P + \overline{M} \otimes Q\right)V^{\dagger}$ such that:

i. There exists an encoding $\tilde{\mathcal{E}}(M) = \tilde{V}\left(M \otimes P + \overline{M} \otimes Q\right) \tilde{V}^{\dagger}$ such that $\tilde{V}\mathbb{1}\tilde{V}^{\dagger}$ is the projector into the low $(<\Delta)$ energy subspace of H_{sim} and $\left\|\tilde{V} - V\right\|_{\infty} \leq \eta$

ii.
$$\|(H_{\text{sim}})_{\leq \Delta} - \tilde{\mathcal{E}}(H_{\text{target}})\|_{\infty} \leq \epsilon$$

We say that a family \mathfrak{F}' of Hamiltonians can simulate a family \mathfrak{F} of Hamiltonians if, for any $H_{\mathrm{target}} \in \mathfrak{F}$ and any $\eta, \epsilon > 0$ and $\Delta > \|H_{\mathrm{target}}\|$ there exists $H_{\mathrm{sim}} \in \mathfrak{F}'$ such that H_{sim} is a (Δ, ϵ, η) -simulation of H_{target} .

This definition has three parameters describing the approximation in the simulation. The physics of the target system is encoded in the subspace of $H_{\rm sim}$ with energy less than Δ , the high energy subspace simulator Hamiltonian contributes inaccuracies to the physics observed, hence in good simulations Δ is taken large to minimise these effects. η describes the error in the eigenstates since the local encoding describing the simulation does not map perfectly into the low energy subspace but instead is close to a general encoding that does. Finally ϵ describes the error in the eigenspectrum, a simple consequence of (ii) is that the low energy spectrum of the simulator is ϵ -close to the spectrum of the target. Given small ϵ and η , the eigenspectrum and corresponding states of the target are well approximated by the simulator. In [CMP19] it is shown that approximate simulations preserve important physical quantities up to controllable errors:

Lemma 6 ([CMP19, Lem. 27, Prop. 28, Prop. 29]). Let H act on $(\mathbb{C}^d)^{\otimes n}$. Let H' act on $(\mathbb{C}^{d'})^{\otimes m}$, such that H' is a (Δ, η, ϵ) -simulation of H with corresponding local encoding $\mathcal{E}(M) = V(M \otimes P + \overline{M} \otimes Q)V^{\dagger}$. Let $p = \operatorname{rank}(P)$ and $q = \operatorname{rank}(Q)$. Then the following holds true.

- i. Denoting with $\lambda_i(H)$ (resp. $\lambda_i(H')$) the i^{th} -smallest eigenvalue of H (resp. H'), then for all $1 \le i \le d^n$, and all $(i-1)(p+q) \le j \le i(p+q)$, $|\lambda_i(H) \lambda_j(H')| \le \epsilon$.
- ii. The relative error in the partition function evaluated at β satisfies

$$\frac{|\mathcal{Z}_{H'}(\beta) - (p+q)\mathcal{Z}_{H}(\beta)|}{(p+q)\mathcal{Z}_{H}(\beta)} \le \frac{(d')^{m} e^{-\beta\Delta}}{(p+q)d^{n} e^{-\beta||H||}} + (e^{\epsilon\beta} - 1).$$
(22)

iii. For any density matrix ρ' in the encoded subspace for which $\mathcal{E}(\mathbb{1})\rho' = \rho'$, we have

$$\|\mathbf{e}^{-iH't}\rho'\mathbf{e}^{iH't} - \mathbf{e}^{-i\mathcal{E}(H)t}\rho'\mathbf{e}^{i\mathcal{E}(H)t}\|_{1} \le 2\epsilon t + 4\eta. \tag{23}$$

Families of Hamiltonians which are able to simulate arbitrary Hamiltonians are called universal:

Definition 7 (Universal Hamiltonians [CMP19, Def. 26]). We say that a family of Hamiltonians is a universal simulator—or simply is universal—if any (finite-dimensional) Hamiltonian can be simulated by a Hamiltonian from the family.

As we will see in the next section, a very good universal simulator for breaking PBQC could simulate arbitrary target Hamiltonians for long times, with small errors, without blowing up the norm of the Hamiltonian.⁹ We can formalise this as:

Definition 8 (Very good universal simulators). We say that a universal family of O(1)-local Hamiltonians M is a very good universal simulator if for any target Hamiltonian H_{target} acting on n spins with locality $\mathcal{L}(n)$ there exists a simulator Hamiltonian $H_{\text{sim}} = \sum_x h_x \in \mathcal{M}$ which is a (Δ, ϵ, η) -simulation of H_{target} where:

$$\max_{i} \|h_{i}\| = \mathsf{poly}\left(\frac{\mathcal{L}^{a}}{\epsilon^{b}} \|H_{\mathsf{target}}\|, \frac{\mathcal{L}^{x}}{\epsilon^{y} \eta^{z}} \|H_{\mathsf{target}}\|\right)$$
(24)

where $a + b \le 1$ and $x + y + z \le 1$.

⁹These requirements would also make a very good simulator for practical applications, with the additional requirement that there it is important that the number of spins in the simulator system doesn't increase too much.

We can also considering loosening the above definition, to the case where we are only interested in target Hamiltonians that belong to some particular family of Hamiltonians:

Definition 9 (Very good $\mathcal{M}_{\text{target}}$ simulators). We say that a universal family of O(1)-local Hamiltonians \mathcal{M} is a very good $\mathcal{M}_{\text{target}}$ simulator if sfor a target Hamiltonian $H_{\text{target}} \in \mathcal{M}_{\text{target}}$ acting on n spins with locality $\mathcal{L}(n)$ and norm $||H_{\text{target}}|| = O\left(\frac{1}{n}\right)$ there exists a simulator Hamiltonian $H_{\text{sim}} = \sum_{x} h_x \in \mathcal{M}$ which is a (Δ, ϵ, η) -simulation of H_{target} where:

$$\max_{i} \|h_{i}\| = \mathsf{poly}\left(\frac{\mathcal{L}^{a}}{\epsilon^{b}} \|H_{\mathrm{target}}\|, \frac{\mathcal{L}^{x}}{\epsilon^{y} \eta^{z}} \|H_{\mathrm{target}}\|\right)$$
(25)

where $a + b \le 1$ and $x + y + z \le 1$.

3.3 PBQC attack from causal toy models

In order to construct an attack on PBQC we will set up an asymptotic quantum task in the causal toy model with the features described in Section 3.1.1. The task is defined by a number of input $\{i_x\}$ and output $\{o_x\}$ points on the boundary of the toy model, a time T_{task} and a unitary U. The task is completed successfully if quantum systems that are input at positions $\{i_x\}$ at time t=0 are acted on by the unitary U and received at positions $\{o_x\}$ at time T_{task} .

We will design the configuration in such a way that the unitary U can be applied locally in the bulk, but cannot be applied locally in the boundary. The set up is shown in Fig. 6 for (2+1)D and (3+1)D systems. The input and output points in both cases are on extreme points of the boundary. This ensures that in the bulk the fastest way to carry out the task is to bring the input quantum systems to the centre of the bulk, apply the unitary, and send them to the output points. The time taken for a signal to travel from the boundary into the centre of the bulk and out to a (possibly different) boundary point is given by $Cn\tau^R$ for some constant C. Applying the bulk unitary will take some non-zero time so we require $T_{\text{task}} > Cn\tau^R$ in order to apply the unitary locally in the bulk. For the configuration shown in Fig. 6 it takes time $\frac{5}{4}Cn\tau^R$ to bring the input quantum systems together and send them to the output quantum systems if we restrict our protocol to only using the boundary. Therefore, to ensure that there is no local boundary protocol for completing the task we require that $T_{\text{task}} < \frac{5}{4}Cn\tau^R$ This means, we can allow bulk computations which run for time $t_U < \frac{1}{4}Cn\tau^R$ so that there is a local bulk procedure but only non-local boundary procedures.

By the end of this section we will have proven the following result:

Theorem 14 (PBQC and simulation). If PBQC is secure against upper bounded linear attacks (Definition 3) then very good universal simulators (Definition 8) cannot exist.

3.3.1 Entanglement in the boundary

We will first demonstrate that the implementation of the n-qubit unitary through the non-local boundary protocol relies on a limited entanglement resource, specifically the boundary state.

As illustrated in Fig. 7, due to causality constraints the boundary protocol can be restricted to two rounds of operations. The boundary regions V, W, V' and W' are defined in Fig. 7 by the inputs/outputs they are causally connected to. The first round of operations take place in V and W separately and a second round of operations in V' and W' with communication allowed in between. Therefore, the amount of entanglement used in the boundary protocol can be captured by the mutual information between the two pairs of boundary regions I(V:W) and I(V':W'). By virtue of time reversal symmetry, these quantities are equal. We will show that in the protocol where a local unitary on n qubits is performed in the bulk, that the mutual information between these regions is upper bounded by

$$I(V:W) \le \frac{1}{2}C_1 n,\tag{26}$$

for some constant $C_1 \ge 4\log(2)R$.

Mutual information is given by the difference in von-Neumann entropies,

$$I(V:W) = S(\rho_V) + S(\rho_W) - S(\rho_{V \cup W}). \tag{27}$$

Hence in order to upper bound the mutual information we need to both upper and lower bound the entropy of a boundary subregion. [Pas+15] section 4 details entropy bounds for perfect tensor networks. We first re-derive an upper bound using results from [Pas+15] to encompass the case where the tensor network is contracted with an entangled bulk state.

First we rephrase a general tensor network result to make use of subsequently:

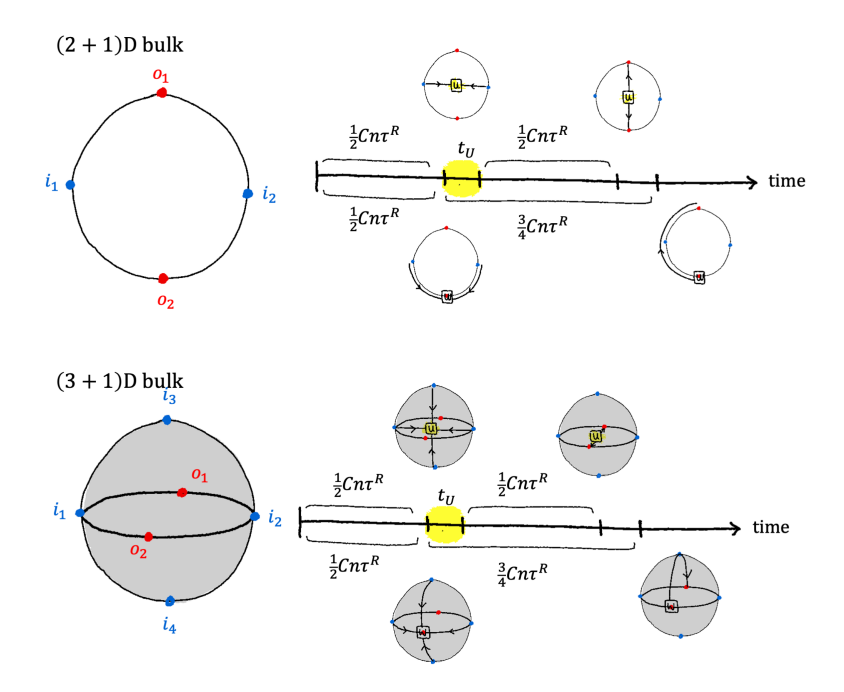


Figure 6: The time for the local bulk computation is limited to $\frac{1}{4}Cn\tau^R$ otherwise a local spacetime region exists on the boundary. Top: a spacelike slice of (2+1)D bulk with inputs and outputs positioned on extreme points in the boundary. The minimum time taken for a particle to travel through the bulk is $Cn\tau^R$. Whereas the minimum time for the inputs to come together on the boundary and then travel to the outputs is $\frac{5}{4}Cn\tau^R$. Therefore, in the bulk a local unitary can be applied on the inputs for time $t_U \leq \frac{1}{4}Cn\tau^R$ while even an instantaneous local boundary protocol is causally impossible. Bottom: the same argument depicted with a (3+1)D bulk.

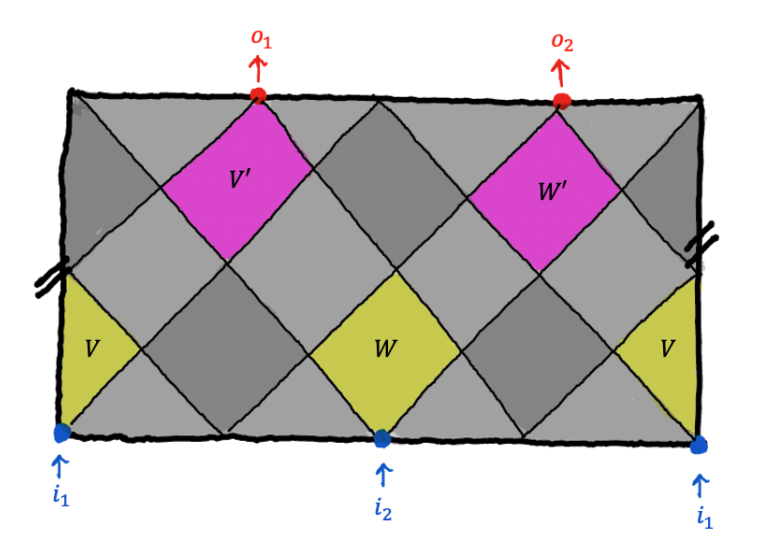


Figure 7: Entanglement regions of interest on the boundary. The boundary regions are defined as follows: V is the intersection of the forward lightcone of i_1 and the backwards lightcones of both outputs; W is the intersection of the forward lightcone of i_2 and the backwards lightcones of both outputs; V is the intersection of the backward lightcone of o_1 and the forward lightcones of both inputs; W' is the intersection of the backward lightcone of i_1 and the forward lightcones of both inputs.

Lemma 10 (General tensor network state entanglement upper bound). Given a tensor network state, $|\psi\rangle$ in \mathcal{H} and a subspace associated with some tensor legs $\mathcal{H}_A \subset \mathcal{H}$. The entanglement entropy is upper bounded by

$$S(\rho_A) \le \min_{\gamma_A} \log d_i, \tag{28}$$

where γ_A is a cut through the tensor network separating \mathcal{H}_A and $\mathcal{H}/\mathcal{H}_A$ that defines a decomposition

of the tensor network into a contract of two tensors P and Q such that,

$$|\psi\rangle = \sum_{a,b,i} P_{ai} Q_{ib} |a\rangle |b\rangle,$$
 (29)

with $|a\rangle$, $|b\rangle$ an orthogonal basis of \mathfrak{H}_A and $\mathfrak{H}/\mathfrak{H}_A$ respectively. d_i is the Hilbert space dimension associated with the contraction between P and Q.

Proof. The reduced density matrix on subsystem \mathcal{H}_A is given by,

$$\rho_A = \operatorname{tr}_{\mathcal{H}/\mathcal{H}_A} \left[|\psi\rangle \langle \psi| \right] \tag{30}$$

$$= \operatorname{tr}_{\mathcal{H}/\mathcal{H}_A} \left[\sum_{a,b,i,a',b',i'} P_{ai} Q_{ib} (Q_{i'b'})^{\dagger} (P_{a'i'})^{\dagger} |a\rangle \langle a'| \otimes |b\rangle \langle b'| \right]$$
(31)

$$= \sum_{a,b,i,a',b',i'} P_{ai}Q_{ib}\overline{Q}_{b'i'}\overline{P}_{i'a'}|a\rangle \langle a'| \otimes \sum_{w} \langle w|b\rangle \langle b'|w\rangle$$
(32)

$$= \sum_{a,b,i,a',i'} P_{ai} Q_{ib} \overline{Q}_{bi'} \overline{P}_{i'a'} |a\rangle \langle a'|, \qquad (33)$$

where $|a\rangle$ is an orthonormal basis for \mathcal{H}_A , $|b\rangle$ and $|w\rangle$ are orthonormal basis for $\mathcal{H}/\mathcal{H}_A$ and overline denotes taking the complex conjugate. The Schmidt rank of ρ_A is the number of strictly positive coefficients, α_j , in the Schmidt decomposition, $\rho_A = \sum_j \alpha_j |a\rangle \langle a|$. From Eq. (33) one can see that the rank of ρ_A is upper bounded by the number of terms in the sum over i,

$$Rank[\rho_A] \le d_i. \tag{34}$$

The von Neumann entropy is upper bounded by log of the rank, hence for all choices of γ_A ,

$$S(\rho_A) \le d_i. \tag{35}$$

To obtain the tightest upper bound minimise over the different choices of γ_A .

We use the above to show a general entropy upper bound for a perfect tensor network HQECC contracted with an entangled bulk state:

Lemma 11 (Boundary entropy upper bound). Given a tensor network HQECC with bond dimension ν , where each tensor has one uncontracted leg associated with bulk degrees of freedom, \mathfrak{H}_{bulk} , and at some finite radius the tessellation is truncated with dangling legs associated with boundary degrees of freedom, $\mathfrak{H}_{boundary}$. Contract the bulk degrees of freedom with a fixed bulk state $|\Psi\rangle_{bulk}$ defining a boundary state $|\Phi\rangle \in \mathfrak{H}_{boundary}$.

For any boundary subregion $\mathcal{H}_A \subset \mathcal{H}_{boundary}$ the entropy of $\rho_A = \operatorname{tr}_{\mathcal{H}_{boundary}/\mathcal{H}_A}[|\Phi\rangle \langle \Phi|]$ is upper bounded by,

$$S(\rho_A) \le \log(\nu)|\gamma_A| + S_{\text{bulk,max}}^a. \tag{36}$$

Where γ_A is the shortest cut anchored at A through the tensor network with a product bulk state contracted on the bulk degrees of freedom. The length of the cut is defined by the number of tensor legs crossed and $|\gamma_A|$ denotes the length of the cut γ_A . Denote by $\mathfrak{H}_a \subset \mathfrak{H}_{\text{bulk}}$ the region of the bulk bounded by A and γ_A . Let the entanglement in the bulk state across the partition, \mathfrak{H}_a , be upper bounded by $S(\operatorname{tr}_{a^c}|\Psi\rangle\langle\Psi|_{\text{bulk}}) \leq S_{\text{bulk,max}}^a$, where $S_{\text{bulk,max}}^a$ is the max-entropy.

Proof. Begin by assuming $S^a_{\text{bulk,max}} = 0$ and the tensor network is contracted with a product bulk state, we call this boundary state $|\tilde{\Phi}\rangle$. Then by Lemma 10 the entropy is upper bounded by, $S(\tilde{\rho}_A) \leq d_i = \log \nu |\gamma_A|$ where minimising γ_A defines a partition of the tensor network into a contraction between two tensors P and Q.

We can then allow $S^a_{\mathrm{bulk,\ max}} > 0$, keeping the same partition γ_A from the product bulk state. Given the information about the entanglement of the bulk state for the partition corresponding to the cut γ_A , the state can be written as $|\Psi\rangle_{\mathrm{bulk}} = \sum_{p,q,j} S_{pj} R_{jq} |p\rangle |q\rangle$, where $\{|p\rangle |q\rangle\}$ is an orthonormal basis spanning $\mathcal{H}_{\mathrm{bulk}}$ and S and R are tensors connected by $S^a_{\mathrm{bulk,\ max}}/\log(2)$ qubit indices. We then redefine a tensor network with P'_{a,i_1,i_2} and Q'_{b,i_1,i_2} corresponding to $P_{a,i_1,j}S_{j,i_2}$ and $Q_{b,i_1,j}R_{j,i_2}$ respectively, see Fig. 8 for reference. Then reusing, Lemma 10 we arrive at the upper bound in the result. Note we are no longer convinced that this is the tightest upper bound, given more information about the geometry of the HQECC there may be a shorter cut.

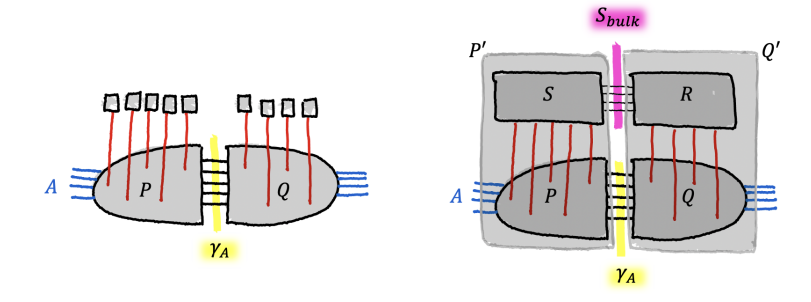


Figure 8: Left) A depiction of $|\tilde{\Phi}\rangle$. A product bulk state in contracted on the HQECC, bulk degrees of freedom are red and boundary degrees of freedom are blue. The boundary subregion A has been selected (although this is general so could be disconnected), and the minimal cut through the network γ_A has been identified defining a partition of the network into the contraction between two tensors P and Q. Right). A depiction of $|\Phi\rangle$. Now the entangled bulk state is contracted $|\Psi\rangle_{\text{bulk}} = \sum_{p,q,j} S_{pj} R_{jq} |p\rangle |q\rangle$ which has been written as a contraction of $S_{\text{bulk, max}}^a/\log(2)$ qubit tensor indices between two tensors S and R. This allows us to define a new tensor network partition P' and Q' and use Lemma 10 to arrive at the result.

The entropy lower bound given in [Pas+15] is shown for product bulk states or holographic states. However, since an entangled bulk state can only generate additional contributions to entanglement, the same lower bound is valid. The result is given in terms of greedy geodesics.

Definition 12 (Greedy algorithm: see [Pas+15]). Start with a cut through a tensor network. One step of the algorithm consists of identifying a tensor for which the current cut crosses at least half of its legs. The update then moves the cut to include this tensor. This procedure is iterated until arriving at the local minimum cut where adding or removing any single tensor does not reduce the cut length.

Figure 7 of [Pas+15] demonstrates that the greedy algorithm can fail to find matching minimal geodesics starting from a boundary region γ_X^* and the complementary boundary region $\gamma_{X^c}^*$. For example, in a model with negative curvature, the algorithm leaves residual bulk regions between γ_X^* and $\gamma_{X^c}^*$ for disconnected regions or connected regions with free bulk indices.

Lemma 13 (Boundary entropy lower bound: see Theorem 3 of [Pas+15]). Given a HQECC contracted from perfect tensors with bond dimension ν . For a holographic state or code with arbitrary bulk state contracted, if A is a (not-necessarily-connected) boundary region and A^c is its complement, then the entropy of the reduced boundary state on A satisfies,

$$\log(\nu)|\gamma_A^{\star} \cap \gamma_{A^c}^{\star}| \le S(\rho_A),\tag{37}$$

where γ_A^* is the greedy geodesic obtained by applying the greedy algorithm to A and $\gamma_{A^c}^*$ is the greedy geodesic obtained by applying the greedy algorithm to A^c .

Proof. See [Pas+15] section 4.2.
$$\Box$$

By Lemma 11 and Lemma 13 the entropy of a boundary subregion X with the bulk state with entanglement S_{bulk} is upper and lower bounded by,

$$\log(\nu)|\gamma_X^{\star} \cap \gamma_{X^c}^{\star}| \le S(\rho_X) \le \log(\nu)|\gamma_X| + S_{\text{bulk,max}}^x. \tag{38}$$

Substituting appropriately from Eq. (38) into Eq. (27) gives the following upper bound on the mutual information,

$$I(V:W) \le \log(\nu) \left[|\gamma_V| + |\gamma_W| - \left| \gamma_{V \cup W}^{\star} \cap \gamma_{(V \cup W)^c}^{\star} \right| \right] + S_{\text{bulk,max}}^v + S_{\text{bulk,max}}^w.$$
(39)

We can use information of our protocol to quantify these contributions to the bounds. For our protocol the bulk state $|\Psi\rangle_{\text{bulk}}$ for the first half of the protocol consists of $|0\rangle\otimes\cdots\otimes|0\rangle$ everywhere except the two inputs i_1 and i_2 consisting of $\lfloor n/2 \rfloor$ qubits each which in general may be entangled. The maximum entanglement in the bulk state is across a partition which contains only one input/output and is given by $\lfloor n/2 \rfloor \log(2)$. Hence $S^v_{\text{bulk,max}}, S^w_{\text{bulk,max}} \propto n$ since these are such partitions, Fig. 9. An equivalent argument gives the same conclusions for V' and W'

since for the second half of the protocol the bulk state $|\Psi\rangle_{\rm bulk}$ consists again of the vacuum everywhere except the two outputs o_1 and o_2 . Note that even if the inputs are promised to be unentangled such that $S^v_{\rm bulk,max}, S^w_{\rm bulk,max} = 0$, the local operation may be entangling so we must take $S^{v'}_{\rm bulk,max}, S^{w'}_{\rm bulk,max} \propto n$.

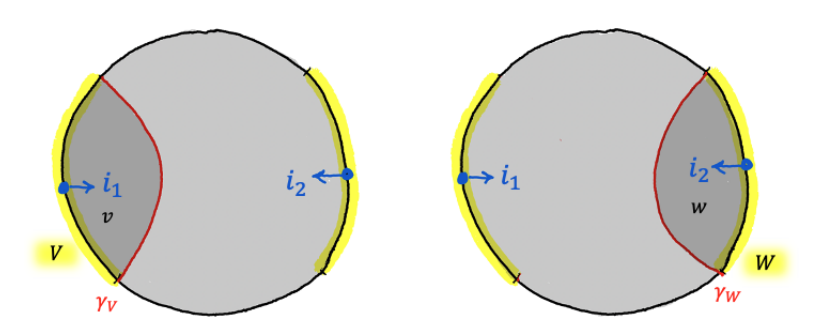


Figure 9: Bulk subregions containing only one input/output have bulk entropy upper bounded by $\lfloor n/2 \rfloor \log(2)$. An equivalent picture exists for V' and W'.

The quantities $|\gamma_V|$, $|\gamma_W|$, $|\gamma_{V\cup W}^{\star}\cap\gamma_{(V\cup W)^c}^{\star}|$ appearing in Eq. (39) are all lengths of cuts through the tensor network. In our network each "tensor leg" actually consists of a bundle of n qubits, hence all lengths are clearly proportional to n.

In the case where the greedy algorithm fails maximally $0 \leq \left| \gamma_{V \cup W}^{\star} \cap \gamma_{(V \cup W)^c}^{\star} \right|$, in this case the lower bound in Lemma 13 simply corresponds to entropy being a non-negative function. Hence,

$$I(V:W) \le \log(2) (|\gamma_V| + |\gamma_W| + n).$$
 (40)

Define $|\Gamma_X| := \frac{1}{n} |\gamma_X|$ as the number of index bundles crossed by cut γ , so that,

$$I(V:W) \le \log(2) (|\Gamma_V| + |\Gamma_W| + 1) n.$$
 (41)

Therefore:

$$I(V:W) \le \frac{1}{2}C_1 n,\tag{42}$$

for some constant independent of n, $C_1 = 2\log(2)(|\Gamma_V| + |\Gamma_W| + 1)$, and equivalently for V' and W'. The cuts through the network can be loosely upper bounded by $|\Gamma_V|, |\Gamma_W| \leq 2R$ - since this cut goes to the centre of the bulk and returns to the boundary, therefore

$$I(V:W) \le \log(2)(2R+1)n.$$
 (43)

The total entanglement for the non-local protocol is then $I(V:W) + I(V':W') \leq C_1 n$ with $C_1 \geq 4 \log(2)R > 1$.

We propose that there is also a matching lower bound which we motivate in Appendix A so that

$$C_0 n \le I(V:W) \le C_1 n,\tag{44}$$

for some constants C_0 , C_1 with $C_0 \leq C_1$. If these arguments could be formalised the mutual information would be bounded from above and below by something proportional to n. However, for the proof of Theorem 14 we only require the upper bound on entanglement.

3.3.2 Proof of main theorem

We are now in a position to prove the main result.

Theorem 14 (PBQC and simulation). If PBQC is secure against upper bounded linear attacks (Definition 3) then very good simulators (Definition 8) cannot exist.

Proof. Let \mathcal{A} be the statement that position based quantum cryptography is secure against upper bounded linear attacks. Let \mathcal{B} be the statement that very good universal simulators exist. The above theorem is then summarised by $\mathcal{A} \implies \neg \mathcal{B}$. Proof by contrapositive, we will show that if very good universal simulators do exist (\mathcal{B}) then we construct a non-local attack on the PBQC protocol implementing a general unitary on n qubits using at most $C_1 n$ entanglement $(\neg \mathcal{A})$.

Consider a tensor network toy model of AdS/CFT with a (2+1)D bulk and a (1+1)D boundary as outlined in the previous section. Set up two input points, i_1, i_2 , at opposite points on the boundary, and two output points o_1, o_2 at spatial positions rotated by $\frac{\pi}{2}$ (see Fig. 10). Consider sending two quantum states, each on $\frac{n}{2}$ qubits, into the bulk from the input points, applying a general unitary U to the pair of inputs when they reach the centre of the tensor network, before sending the resulting state to the two outputs.

In order to ensure that the boundary dynamics for this evolution gives a protocol for non-local quantum computation we require that the bulk unitary is applied for time at most $t_U < \frac{C}{4}n\tau^R$ to prevent a local region existing in the boundary (see Fig. 6). We must also take R large enough so that the inputs and outputs are disjoint on the bulk and boundary theory and the size of the inputs on the boundary are negligible with respect to traversing the boundary to ensure that the constants in the analysis do not change the causal structure of the boundary.

On the boundary while the inputs are non-interacting we simply evolve the boundary under the bulk Hamiltonian pushed out through the tensor network to the boundary. The bulk Hamiltonian at this stage is not the Hamiltonian that implements the unitary U, it is simply a Hamiltonian that moves the input quantum state into the bulk – i.e. a time-dependent bulk Hamiltonian that implements a SWAP operation on the states' current position in the tensor network, and the next tensor in the path. There is a choice of how this bulk Hamiltonian is pushed out to the boundary – we will adopt the 'natural' choice of pushing directly out towards the boundary. This minimises the portion of the boundary which is needed to reconstruct each input. Crucially, since each input can be wholly reconstructed on the portion of the boundary being used, by the no-cloning theorem there can be no information about input 1 on the portion of the boundary used to reconstruct input 2, or vice versa. These interactions acts on large portions of the boundary at once, but it is non-interacting between the two portions of the boundary used to reconstruct each input, and does not evolve signals faster than the butterfly velocities outlined in the previous section, so respects the causality constraints.

When the unitary U is applied in the centre of the bulk we cannot simply use the bulk Hamiltonian pushed through the tensor network on the boundary. This is because for general unitaries the interaction is non-separable over the two relevant portions of the boundary, so the boundary unitary would also be non-causal in the sense of acting on both inputs simultaneously. However, let $U=e^{iH_{\rm target}t}$ where $t\leq n\tau^R$, and $H_{\rm target}$ is some general Hamiltonian acting on n qubits, satisfying $\|H_{\rm target}\|=\frac{\tau^{-R}}{n}$. To construct $H_{\rm target}$ from U we simply take the principal branch of the matrix logarithm. Pushed out to the boundary $H_{\rm target}$ will be some $n\tau^R$ -local Hamiltonian $H_{\rm boundary}$, with norm $\|H_{\rm boundary}\|=\frac{\tau^{-R}}{n}$ since the bulk-boundary tensor network mapping is an isometry. By assumption, there exists Hamiltonian simulation techniques to construct a Hamiltonian $H=\sum_i h_i$ which is a (Δ,ϵ,η) -simulation of an arbitrary Hamiltonian $H_{\rm target}$ acting on N qubits where:

$$\max_{i} \|h_{i}\| = \mathsf{poly}\left(\frac{\mathcal{L}^{a}}{\epsilon^{b}} \|H_{\text{target}}\|, \frac{\mathcal{L}^{x}}{\epsilon^{y} \eta^{z}} \|H_{\text{target}}\|\right)$$
(45)

where $a+b \leq 1$ and $x+y+z \leq 1$. We require $\epsilon t \ll 1$ so that the error in the simulation is small – so we set $\epsilon = O\left(\frac{\tau^{-R}}{n}\right)$. The locality of our initial Hamiltonian is $\mathcal{L} = n\tau^R$, so we find that $\frac{\mathcal{L}^a}{\epsilon^b} = O\left((n\tau^R)^{a+b}\right)$. By setting $\|H_{\text{target}}\| = \frac{\tau^{-R}}{n}$ we find $\frac{\mathcal{L}^a}{\epsilon^b} \|H_{\text{target}}\| = O(1)$. Moreover, this gives us a 'computation budget' of $\|H_{\text{target}}t\| = O(1)$ that is able to generate an arbitrary unitary on n qubits. To keep the error in the simulation small we also require that $\eta \ll 1$. We will let $\eta = \frac{1}{n\tau^R} \ll 1$. This can be achieved without blowing up the interaction strength provided $\frac{\mathcal{L}^x \|H_{\text{target}}\|}{\epsilon^y \eta^z} = O(1)$. Substituting in the values we require that $(n\tau^R)^{x+y+z-1} = O(1)$, which is true since by assumption $x+y+z \leq 1$. Consequently, this simulation exhibits a local interaction strength of $\max_i \|h_i\| = O(1)$.

After the unitary has been applied in the centre of the bulk, the two outputs are sent to the output points on the boundary. Again here we can evolve on the boundary using the non-local (but non-interacting between the two outputs) Hamiltonian which results from pushing the Hamiltonian directly through the tensor network.

The boundary protocol outlined above that implements the simulated Hamiltonian acts over the entire boundary. When the inputs are propagating into the centre of the bulk and back out to the boundary, the boundary Hamiltonian is causal from butterfly velocities. Additionally when the local unitary is being applied in the bulk the simulated boundary Hamiltonian is geometrically local by construction. Therefore, since the protocol is causal at every point signals on the boundary

¹⁰This ensures that the 'computation budget' $H_{\text{target}}t = O(1)$ so we can implement general unitaries.

cannot be travelling outside the causal light cones defined by the butterfly velocities and the Lieb-Robinson velocities. As a result we can choose to apply all the boundary steps of the protocol in the V, W, V', W' portions of the boundary shown in Fig. 7, and trace out all other regions of the boundary.

As outlined in Section 3.3.1 the entanglement between these regions is upper-bounded by C_1n for some constant $C_1 \geq 4\log(2)R$. Therefore, if very good simulations exist, such that \mathcal{B} is true, we can construct a non-local attack on position-based quantum cryptography with an error in the final state of $\epsilon t + \eta \ll 1$ using at most linear entanglement by using the HQECC and Hamiltonian simulation techniques to transform the local bulk protocol into a non-local boundary one that implements the same task.

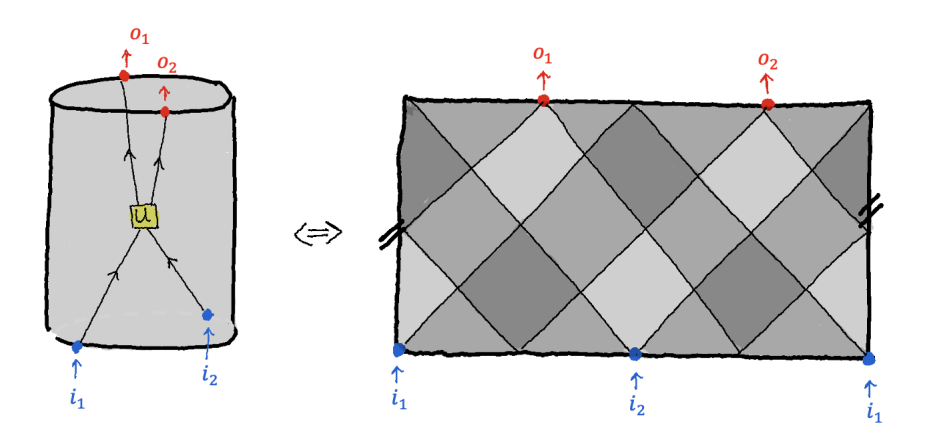


Figure 10: The set up for our holography inspired proof of Theorem 14.

Theorem 14 holds for general unitaries. However, we can derive a corollary by restricting the local unitary in the position-based protocol to those generated by certain families of Hamiltonians. This demonstrates that even when considering a limited family of unitaries the same logic bounds the interaction strength of the simulator Hamiltonian:

Corollary 15 (PBQC and simulation). If every PBQC that implements a unitary $U = e^{iH_U t}$ for $H_U \in \mathcal{M}_U$ is secure against upper bounded linear attacks (Definition 3) then very good \mathcal{M}_{target} simulators (Definition 9) cannot exist, where \mathcal{M}_U and \mathcal{M}_{target} are related by an isometry.

Proof. This follows immediately from the proof of Theorem 14, where instead of allowing the unitary implemented in the bulk to be general, we require that is generated by a restricted family of Hamiltonians (e.g. k-local Hamiltonians). The form of the H_{target} comes from pushing the Hamiltonian that generates the unitary through the tensor network, as outlined in the proof of Theorem 14.

See Section 4 for more discussion on these results.

3.4 Best known simulation techniques

In order to assess the importance of the lower bound on resources required for simulation from Theorem 14 we can compare it to the current best known simulation techniques.

In Appendix B we modify the universal Hamiltonian construction of [Koh+20] to one where the interactions themselves depend on the Hamiltonian to be simulated (in a precise manner). In this way we are able to exponentially improve on the required interaction strength in the simulator system. However, for general Hamiltonians this only takes us from a doubly exponential scaling of interaction strength with N to a single exponential scaling. This is clearly significantly worse than the optimum scaling outlined in Theorem 14. However, when restricting to sparse Hamiltonians we are able to construct a family of 2-local Hamiltonians $H = \sum_i h_i$ which can simulate an arbitrary sparse Hamiltonian H_{target} with interaction strength satisfying $\max_i \|h_i\| = \left(\text{poly}\left(\frac{N^a}{\epsilon^b}\|H_{\text{target}}\|,\frac{N^x}{\epsilon^y\eta}\|H_{\text{target}}\|^z\right)\right)$ where $a+b>1\frac{1}{2}$ and $x+y+z>1\frac{3}{4}$.¹¹

¹¹ For target Hamiltonians that are O(1)-sparse we can achieve $a+b=1\frac{1}{2}$ and $x+y+z=1\frac{3}{4}$. For more general poly(N) sparse Hamiltonians we can achieve $a+b>1\frac{1}{2}$ and $x+y+z>1\frac{3}{4}$ where the exact values depend on the degree of the polynomial.

Note that when considering the result about sparse Hamiltonians in the setting of Corollary 15 it is H_{target} which we require to be sparse. A sufficient condition for H_{target} to be sparse is that the Hamiltonian generating the unitary in the PBQC protocol have Pauli rank $O(\mathsf{poly}(n))$ (where the Pauli rank is the number of terms in the Pauli decomposition of the Hamiltonian). This set of Hamiltonians includes, but is not limited to, k-local Hamiltonians for constant k.

Although the achievable simulations for sparse Hamiltonians are close to the bounds in Theorem 14, they still do not allow us to construct interesting attacks on PBQC. This is because in order to keep the part of the error that scales with time small we have to focus on very low norm bulk Hamiltonians. However, this means that the unitary we are carrying out is close to the identity, and its simulation is swamped by the part of the error that is time-independent.

The simulation techniques from Appendix B are non-perturbative. In Section C we investigate perturbative simulation techniques. However, there are no regimes where these give bounds as good as the non-perturbative alternatives. This may be because we have not optimised the perturbative techniques for cases where we are simulating Hamiltonians that have large locality but are sparse. Optimising these types of simulation has been investigated and it has been suggested that they generically require $\max_i \|h_i\| = O\left(\|H_{\text{target}}\|\text{poly}\left(\frac{1}{\epsilon^k}\right)\right)$ to simulate a k-local H_{target} with a 2-local $H = \sum_i h_i$ while keeping the error and the number of spins fixed [Cao+17; Bra+08; CN18]. As in the case of the non-perturbative techniques, any attack on PBQC using these perturbative techniques would only be applicable for the case of a unitary that was close to trivial.

4 Discussion

4.1 Toy models of AdS/CFT

The rescaling of the Hamiltonian in tensor network toy models of AdS/CFT gives toy models with more of the expected causal features of the duality. However, the toy models outlined here are still lacking key features such as Lorentz invariance, and conformal symmetry on the boundary. Understanding whether it is possible to incorporate those other features of AdS/CFT into toy models could help aid our understanding of which features of holography are fundamentally gravitational. Moreover, the time dilation expected in AdS/CFT does not appear naturally in these types of toy models, the way it does in e.g. [Mas23]. Constructing toy models where time dilation appears naturally but which also have bulk degrees of freedom (which [Mas23] does not) remains an open question and would be the ideal tool for understanding PBQC protocols in holography in a toy setting.

4.2 The connection between Hamiltonian simulation and PBQC

To build on our main theorem there are two key areas for future research. The first is attempting to construct simulators which achieve the bounds in Theorem 14. While doing this for completely general Hamiltonians is a daunting task, it may be possible to do for restricted families of Hamiltonians. Indeed, for certain families of sparse Hamiltonians we can already get close to the bounds, although not close enough to construct interesting attacks on PBQC (Appendix B). As highlighted by Corollary 15, constructing simulators that could achieve the bounds from Theorem 14 for restricted families of target Hamiltonians would already demonstrate that there exist certain families of unitaries that cannot be used as the basis for PBQC protocols that are secure against linear entanglement. For example, the families of sparse Hamiltonians we construct simulations for in Appendix B correspond to unitaries which are generated by k-local Hamiltonians. Therefore, if we could close the gap between the results of Appendix B and the bounds in Theorem 14 we would demonstrate that unitaries which are generated by k-local Hamiltonians cannot be used as the basis for PBQC protocols that are secure against linear entanglement. On the other hand, if unitaries generated by k-local Hamiltonians can be used as the basis for PBQC protocols which are secure against linear entanglement this immediately implies that the results in Appendix B are close to optimal for simulating sparse Hamiltonians.

We note that a recent work [Har+23] shows that for modular simulations of a k-local Hamiltonian (i.e. simulations where each k-local term in $H_{\rm target}$ is simulated independently by a gadget) the interaction strength of the simulator Hamiltonian can be lower bounded by $O(n^{\frac{1}{2}})$. The no go result in [Har+23] does not apply to simulations where the whole of $H_{\rm target}$ is simulated at once (e.g. history state simulations, see Appendix B) and hence it does not rule out the 'very good' simulations in Theorem 14. They also propose a new definition of dynamical simulation that is weaker than Definition 5 in that it only requires simulating subsets of observables, rather than the entire

state. Within this definition they are able to circumvent their no go result by utilising repeated measurement of ancilla spins to construct a dynamical simulation of a O(1)-local Hamiltonian with O(1) interaction strengths. This technique relies on a Lieb-Robinson type argument to bound the evolution of a very local observable under a Hamiltonian acting on a larger system. The condition that the Hamiltonian is geometrically O(1)-local is necessary in their error bound and therefore cannot be applied to a general Hamiltonian acting on n qubits – as is the case for the boundary Hamiltonian in the toy model – to obtain a PBQC attack.

There are simpler lower bounds on the interaction strengths requires to simulation n local Hamiltonians with geometrically 2 local terms due to causality arguments. We explore these in Appendix D. The bound is linear in n and therefore weaker than that of Theorem 14 due to the exponents (a+b>1). Furthermore, allowing an error in the state does not alter the scaling – a key feature of this result. We leave it to future work to investigate whether causality requirements may produce new simulation lower bounds.

If there are states with no long-range entanglement in the simulator subspace then the conditional restrictions on 'very good simulations' can be shown unconditionally via a Lieb-Robinson argument. However, this argument cannot be applied when there is long-range entanglement, as is the case for the position-based cryptography set up with O(n) entanglement between opposite sides of the boundary. It could be possible to simulate a signalling Hamiltonian with a non-signalling Hamiltonian if the large norm difference between operators – which is guaranteed to exist due to Lieb-Robinson bounds – originates from outside the simulator subspace.

Appendices

Appendix A Motivation of matching lower bound for boundary entanglement

In Section 3.3.1 we prove an upper bound on the boundary entanglement between regions used for computation. We propose that there is also a matching lower bound so that

$$C_0 n \le I(V:W) \le C_1 n,\tag{46}$$

for some constants C_0 , C_1 with $C_0 \leq C_1$. In this section we construct an argument for this lower bound.

Again using Lemma 11 and Lemma 13 the mutual information lower bound is

$$\log(\nu) \left[|\gamma_V^{\star} \cap \gamma_{V^c}^{\star}| + |\gamma_W^{\star} \cap \gamma_{W^c}^{\star}| - |\gamma_{V \cup W}| \right] - S_{\text{bulk}}^{\nu \cup w} \le I(V:W), \tag{47}$$

If the bulk partition contains both inputs (or neither) – as is the case for $v \cup w$ – then the bulk state is product over this partition and $S_{\text{bulk}}^{v \cup w} = 0$, Fig. 11.

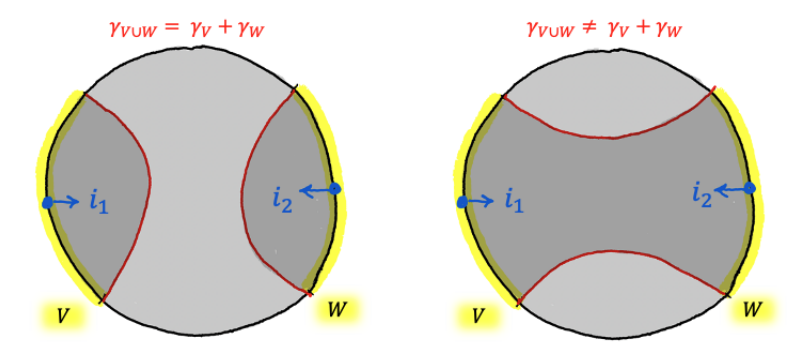


Figure 11: Bulk subregions containing both input/output have bulk entropy equal to 0. An equivalent picture exists for V' and W'. The left depics a disconnected causal wedge

As with the lengths in the upper bound the quantities $|\gamma_V^{\star} \cap \gamma_{Vc}^{\star}|, |\gamma_W^{\star} \cap \gamma_{Wc}^{\star}|, |\gamma_{V \cup W}|$ in Eq. (47) are each proportional to n. The bound is non-trivial if

$$|\gamma_V^{\star} \cap \gamma_{V^c}^{\star}| + |\gamma_W^{\star} \cap \gamma_{W^c}^{\star}| > |\gamma_{V \cup W}|. \tag{48}$$

We conjecture the above equation holds evidenced by the following:

- It was proven that $|\gamma_{V \cup W}| < |\gamma_V| + |\gamma_W|$ (ie a connected wedge as in the right of Fig. 11) for the same asymptotic task set up using quantum information theoretic tools via the B_{84} in [May19], which was then refined and also argued via classical general relativity in [MPS19]. We conjecture that the same result will hold for tensor networks.
- $|\gamma_V^* \cap \gamma_{V^c}^*| = |\gamma_V^*|$ if there is no residual region for V, i.e. V is not a 'pathogenic' boundary region. A boundary region is pathogenic if there exits some bulk operation that cannot be recovered on the region or its complement. Given the freedom to chose Coxeter polytopes with different numbers of faces and rotate the region V around the boundary, we argue that this can always be avoided. Hence it is possible to construct a tensor network PBQC protocol such that $|\gamma_V^* \cap \gamma_{V^c}^*| = |\gamma_V^*| = |\gamma_V|$.

Appendix B An explicit non-perturbative construction of an attack on PBQC

In [Koh+20] a "history-state method" for Hamiltonian simulation was outlined. This simulation technique leverages the ability to encode computation into ground states of local Hamiltonians via computational history states. A computational history state $|\Phi\rangle_{CQ}\in\mathcal{H}_C\otimes\mathcal{H}_Q$ is a state of the form

$$|\Phi\rangle_{CQ} = \frac{1}{\sqrt{T}} \sum_{t=1}^{T} |t\rangle |\psi_t\rangle \,,$$

where $\{|t\rangle\}$ is an orthonormal basis for \mathcal{H}_C and $|\psi_t\rangle = \prod_{i=1}^t U_i |\psi_0\rangle$ for some initial state $|\psi_0\rangle \in \mathcal{H}_Q$ and set of unitaries $U_i \in \mathcal{B}(\mathcal{H}_Q)$.

 \mathcal{H}_C is the clock register and \mathcal{H}_Q is the computational register. If U_t is the unitary transformation corresponding to the t^{th} step of a quantum computation (in any model of computation, e.g. quantum circuits, quantum Turing machines, or more exotic models of computation), then $|\psi_t\rangle$ is the state of the computation after t steps. The history state $|\Phi\rangle_{CQ}$ then encodes the evolution of the quantum computation. History state Hamiltonians are constructed so that their ground states are computational history states. In [Koh+20] a method is derived to construct universal Hamiltonians via history state methods. Here we use a slight modification of that method.¹²

We construct a history state Hamiltonian, $H_{\rm PE}$, which encodes the Turing machine model of computation. The input to the Turing machine is a set of 'physical spins' – the state of these spins is left arbitrary; they encode the state of the system being simulated. The computation being encoded is a long period of 'idling' (i.e. doing nothing), followed by quantum phase estimation applied to the the physical spins with respect to the unitary generated by $H_{\rm target}$. The output of the $H_{\rm PE}$ computation is the energy of the physical spins with respect to the Hamiltonian $H_{\rm target}$. This energy is written to the Turing machine tape in the form $E = \|H_{\rm target}\| (m_{\alpha}\sqrt{2} - m_{\beta})$ by writing m_{α} α symbols and m_{β} β symbols to the tape.

The simulator Hamiltonian is then given by:

$$H_{\text{sim}} = JH_{\text{PE}} + T \|H_{\text{target}}\| \sum_{i=0}^{N-1} \left(\sqrt{2}\Pi_{\alpha}^{(i)} - \Pi_{\beta}^{(i)}\right)$$
(49)

where T is the total number of time steps in the computation encoded by $H_{\rm PE}$, N is the number of spins in the simulator system, $\Pi_{\alpha}^{(i)}$ and $\Pi_{\beta}^{(i)}$ are the projectors onto the $|\alpha\rangle$ and $|\beta\rangle$ basis states applied to the $i^{\rm th}$ spin, and J is some large value which pushes all states which have non-zero energy with respect to $H_{\rm PE}$ to high energies. To understand why this Hamiltonian gives a simulation of $H_{\rm target}$ note that $H_{\rm PE}$ has a degenerate zero energy ground space, that is spanned by history states. These history states encode the phase estimation algorithm applied to different states of the physical spins. All other states have very high energies, due to the J factor. The projectors in $H_{\rm sim}$ break the ground space degeneracy of $H_{\rm PE}$ by giving the appropriate energy factors the the $|\alpha\rangle$ and $|\beta\rangle$ spins which encode the output of the phase estimation algorithm.

It follows immediately from [Koh+20, Lemma 4.3] that the Hamiltonian in Eq. (49) is a (Δ, ϵ, η) -simulation of H_{target} with:

$$\eta = O\left(\frac{T^3 \|H_{\text{target}}\|}{J} + \frac{T_{\text{PE}}}{T}\right) \tag{50}$$

¹²In [Koh+20] the aim was to minimise the number of parameters needed to describe a universal quantum simulators. Here we are instead interested in minimising the norm of the simulator interactions. For that reason, instead of encoding the target Hamiltonian in a feature of the simulator system, we instead encode it directly into the interactions.

$$\epsilon = \epsilon' + O\left(\frac{T^4 \|H_{\text{target}}\|^2}{J}\right) \tag{51}$$

$$\Delta = \frac{J}{2T^2} \tag{52}$$

where J and T are as defined in Eq. (49), $T_{\rm PE}$ is the time for the phase estimation part of the history state computation (i.e. $T_{\rm PE} = T - L$ for L the number of idling steps), and ϵ' is the error in the phase estimation computation.

Therefore we will need to select L so that $T \geq \frac{T_{PE}}{\eta}$, giving:

$$J \ge \Delta T^2 + \frac{T^3 \|H_{\text{target}}\|}{\eta} + \frac{T^4 \|H_{\text{target}}\|}{\epsilon}.$$
 (53)

To compare this with the bound in Theorem 14 we need to determine the time needed for the phase estimation algorithm.

B.1 Quantum Phase Estimation computation time

The QPE algorithm requires us to implement the unitary $U = e^{iH_{\text{target}}t_u}$ where $||H_{\text{target}}t_u|| \leq 2\pi$. If we want to estimate the eigenvalues of H_{target} to accuracy ϵ' we need to determine the phase of U to accuracy $\frac{\epsilon'}{||H_{\text{target}}||}$ which requires $\frac{||H_{\text{target}}||}{\epsilon'}$ implementations of U.

Using [BCK15] we can implement a unitary U generated by a d-sparse Hamiltonian which acts on N spins to within accuracy ϵ'' in time

$$T_U = O\left(\kappa \left(1 + N + \log^{\frac{5}{2}} \left(\frac{\kappa}{\epsilon''}\right)\right) \frac{\log\left(\frac{\kappa}{\epsilon''}\right)}{\log\log\left(\frac{\kappa}{\epsilon''}\right)}\right)$$
(54)

where $\kappa = d\|H_{\text{target}}\|_{\text{max}} t_u$. Here $\|H_{\text{target}}\|_{\text{max}}$ denotes the largest entry of H_{target} in absolute value. We will choose t_u so that $\|H_{\text{target}}\|_{\text{max}} t_u = O(1)$, and set $\epsilon'' = \frac{\epsilon'}{\|H_{\text{target}}\|}$ giving

$$T_{U} = O\left(d\left(1 + N + \log^{\frac{5}{2}}\left(\frac{d\|H_{\text{target}}\|}{\epsilon'}\right)\right) \frac{\log\left(\frac{d\|H_{\text{target}}\|}{\epsilon'}\right)}{\log\log\left(\frac{d\|H_{\text{target}}\|}{\epsilon'}\right)}\right).$$
 (55)

Therefore we have that:

$$T_{\text{PE}} = \frac{\|H_{\text{target}}\|}{\epsilon'} T_U = O\left(\frac{d\|H_{\text{target}}\|}{\epsilon'} \left(1 + N + \log^{\frac{5}{2}} \left(\frac{d\|H_{\text{target}}\|}{\epsilon'}\right)\right) \frac{\log\left(\frac{d\|H_{\text{target}}\|}{\epsilon'}\right)}{\log\log\left(\frac{d\|H_{\text{target}}\|}{\epsilon'}\right)}\right). (56)$$

B.2 General simulation bounds

From Eq. (50) we have that,

$$\eta \ge \frac{T_{\rm PE}}{T} = \frac{T_{\rm PE}}{T_{\rm DE} + L}.\tag{57}$$

This follows since η is at least as large as the second term in Eq. (50), and the total time for the computation is given by the time for the phase estimation algorithm plus the idling time.

So we can set $L = \lambda T_{PE}$ for some large constant λ . This gives $T = O(T_{PE})$.

This gives:

$$\eta = O\left(\frac{\|H_{\text{target}}\|^4}{J} \left(\frac{d}{\epsilon'} \left(N + \log^{\frac{5}{2}} \left(\frac{d\|H_{\text{target}}\|}{\epsilon'}\right)\right) \frac{\log\left(\frac{d\|H_{\text{target}}\|}{\epsilon'}\right)}{\log\log\left(\frac{d\|H_{\text{target}}\|}{\epsilon'}\right)}\right)^3 + \frac{1}{m}\right)$$
(58)

$$\epsilon = O\left(\epsilon' + \frac{\|H_{\text{target}}\|^6}{J} \left(\frac{d}{\epsilon'} \left(N + \log^{\frac{5}{2}} \left(\frac{d\|H_{\text{target}}\|}{\epsilon'}\right)\right) \frac{\log\left(\frac{d\|H_{\text{target}}\|}{\epsilon'}\right)}{\log\log\left(\frac{d\|H_{\text{target}}\|}{\epsilon'}\right)}\right)^4\right)$$
(59)

$$\Delta = O\left(\frac{J}{\left(\frac{d\|H_{\text{target}}\|}{\epsilon'}\left(N + \log^{\frac{5}{2}}\left(\frac{d\|H_{\text{target}}\|}{\epsilon'}\right)\right) \frac{\log\left(\frac{d\|H_{\text{target}}\|}{\epsilon'}\right)}{\log\log\left(\frac{d\|H_{\text{target}}\|}{\epsilon'}\right)}\right)^{2}}\right).$$
(60)

Therefore:

$$J = \mathsf{poly}\left(\left(\frac{N^4 d^4}{\epsilon^5}\right)^{\frac{1}{6}} \|H_{\mathrm{target}}\|, \left(\frac{N^3 d^3}{\eta \epsilon^3}\right)^{\frac{1}{4}} \|H_{\mathrm{target}}\|, d^2 \Delta, \log\left(\frac{d \|H_{\mathrm{target}}\|}{\epsilon}\right), \frac{1}{\log\left(\log\left(\frac{d \|H_{\mathrm{target}}\|}{\epsilon}\right)\right)}\right). \tag{61}$$

where we have used that ϵ' is upper bounded by ϵ . Therefore, for d = O(1) this gives a simulation method where $\max_i \|h_i\| = \left(\mathsf{poly}\left(\frac{N^a}{\epsilon^b}\|H_{\mathrm{target}}\|, \frac{N^x}{\epsilon^y\eta^z}\|H_{\mathrm{target}}\|\right)\right)$ where a+b=1.5 and $x+y+z=1\frac{3}{4}$. For polynomially sparse Hamiltonians we have that a+b>1.5 and $x+y+z>1\frac{3}{4}$, where the tightness of the lower bounds depends on the degree of the polynomial in the sparsity. While these are close to the bounds from Theorem 14 for the case of sparse Hamiltonians, for general Hamiltonians the d-factor in Eq. (61) contributes a factor which is exponential in N, and results in a scaling that is far from that in Theorem 14.

B.3 Holographic Quantum Error Correcting Codes using this construction

In this section we investigate using these simulation techniques in the attack on PBQC outlined in the proof of Theorem 14 for general Hamiltonians. In this case we have $N=n\tau^R$. The Pauli rank of the operator to be simulated as at most 4^n so $d=O(4^n)$. Let us set $\|H_{\rm target}\|=\tau^{-\alpha R}4^{-\alpha n}$ and $\epsilon'=\tau^{-\beta R}4^{-\beta n}$ where we require $\beta\geq\alpha>0$ to ensure that the accuracy with which the unitary $U=e^{iH_{\rm target}t_u}$ is implemented is small with respect to $\|H_{\rm target}\|$. We find:

$$T_{\text{PE}} = O\left(n4^{(\beta-\alpha+1)n}\tau^{(\beta-\alpha)R}\left(n\tau^R + ((\beta+\alpha+1)n)^{5/2} + ((\beta-\alpha)R\log\tau)^{5/2}\right) \times \frac{(\beta-\alpha+1)n + (\beta-\alpha)R\log\tau}{\log((\beta+1-\alpha)n + (\beta-\alpha)R\log\tau}\right).$$
(62)

For concreteness let us choose $\beta = \alpha$:

$$T_{\rm PE} = O\left(\frac{4^n (n^2 \tau^R + n^{7/2})}{\log(n)}\right). \tag{63}$$

Giving:

$$\eta = O\left(\frac{4^{(3-\alpha)n}\tau^{-\alpha R}(n^6\tau^{3R} + n^{21/2})}{J\log^3(n)}\right)$$
(64)

$$\epsilon = O\left(\frac{4^{2(2-\alpha)n}\tau^{-2\alpha R}(n^8\tau^{4R} + n^14)}{J\log^4(n)}\right) \tag{65}$$

$$\Delta = O\left(\frac{J\log^2(n)}{4^{2n}(n^2\tau^{2R} + n^7)}\right).$$
 (66)

Therefore if we set J = O(1) as required for causality in the toy model, then we can construct a 'good' simulation in terms of ϵ and Δ (i.e. a simulation where $\epsilon \ll \|H_{\text{target}}\|$ and $\Delta \gg \|H_{\text{target}}\|$) if we choose $\alpha > 4$. For concreteness we will set $\alpha = 5$. This gives:

$$\eta = O\left(\frac{4^{-2n}\tau^{-5R}(n^6\tau^{3R} + n^{21/2})}{\log^3(n)}\right) \tag{67}$$

$$\epsilon = O\left(\frac{4^{6n}\tau^{-10R}(n^8\tau^{4R} + n^{14})}{\log^4(n)}\right)$$
 (68)

$$\Delta = O\left(\frac{\log^2(n)}{4^{2n}(n^2\tau^{2R} + n^7)}\right).$$
 (69)

However, recall that in order to maintain the link to PBQC we can only evolve the system for time $\frac{1}{4}Cn\tau^R$, so in this set-up we can only perform a unitary with "computation budget" at most $\|H_{\text{bulk}}\|_{t} = n4^{-5n}\tau^{-4R}$. From Lemma 6 the error in the state at the end of the simulation would be:

$$\|\mathbf{e}^{-iH_{\text{sim}}t}\rho'\mathbf{e}^{iH_{\text{sim}}t} - \mathbf{e}^{-i\mathcal{E}(H_{\text{target}})t}\rho'\mathbf{e}^{i\mathcal{E}(H_{\text{target}})t}\|_{1}$$

$$\leq O\left(\frac{4^{6n}\tau^{-9R}(n^{7}\tau^{3R} + n^{23/2})}{\log^{4}(n)} + \frac{4^{-2n}\tau^{-5R}(n^{6}\tau^{3R} + n^{21/2})}{\log^{3}(n)}\right). \tag{70}$$

We see that while the ϵ -error is small (and can be made arbitrarily so by reducing the norm of H_{target}), we cannot achieve a error in η which is small with respect to the computation budget without increasing J. While the η error does not accumulate with time it nevertheless dominates the error for the small computation budget we are considering here, and this error swamps the simulation.

B.4 Holographic Quantum Error Correcting Codes using this construction for a restricted class of bulk Hamiltonians

In this section we will examine the results of applying the simulation techniques from Section B.2 in a HQECC set up for bulk Hamiltonians which are k-local for constant k. This guarantees that the target Hamiltonian on the boundary of the HQECC is sparse, therefore from Section B.2 we know that we can get very close to saturating the definition of very good simulators. However, in this section we will see that despite getting very close to the bounds, the simulations do not provide interesting attacks on position based cryptography because the errors in the simulation dominate the computation being carried out.

We still have that $N = n\tau^R$, and now we have d = O(1). Let us set $||H_{\text{target}}|| = \tau^{-\alpha R} n^{-\alpha' k}$ and $\epsilon' = \tau^{-\beta R} n^{-\beta' k}$ where we require $\beta \ge \alpha > 0$ and $\beta' \ge \alpha' > 0$ to ensure that the accuracy with which the unitary $U = e^{iH_{\text{target}}t_u}$ is implemented is small with respect to $||H_{\text{target}}||$. Substituting the above into Eq. (56) we find:

$$T_{\text{PE}} = O\left(n^{(\beta' - \alpha' + 1)k + 1} \tau^{(\beta - \alpha)R} \left(n\tau^{R} + ((\beta' - \alpha' + 1)k\log n)^{5/2} + ((\beta - \alpha)k\log \tau)^{5/2}\right) \times \frac{(\beta' - \alpha' + 1)\log(n) + (\beta - \alpha)R\log(\tau)}{\log((\beta' - \alpha' + 1)\log(n) + (\beta - \alpha)R\log(\tau))}\right).$$
(71)

For concreteness let us choose $\beta = \alpha$ and $\beta' = \alpha'$:

$$T_{\text{PE}} = O\left(\frac{n^k (n\tau^R + \log^{5/2} n) \log(n)}{\log\log(n)}\right)$$
(72)

$$= O\left(\frac{n^{k+1}\tau^R \log(n)}{\log\log(n)}\right). \tag{73}$$

Eq. (61) now implies the following scalings on the simulation parameters:

$$\eta = O\left(\frac{n^{(3-\alpha')k+3}\tau^{(3-\alpha)R}\log^3(n)}{J\log^3(\log(n))}\right)$$
(74)

$$\epsilon = O\left(\frac{n^{2(2-\alpha')k+4}\tau^{2(2-\alpha)R}\log^4(n)}{J\log^4(\log(n))}\right)$$
(75)

$$\Delta = O\left(\frac{J\log^2(\log(n))}{n^{2(k+1)}\tau^{2R}\log^2(n)}\right). \tag{76}$$

Therefore if we set J=O(1) as required for causality in the toy model, and assume k=2 for concreteness, then we can construct a 'good' simulation in terms of ϵ and Δ (i.e. a simulation where $\epsilon \ll \|H_{\text{target}}\|$ and $\Delta \gg \|H_{\text{target}}\|$) if we choose $\alpha'>6$ and $\alpha>4$. For concreteness we will set $\alpha'=7$ and $\alpha=5$. This gives:

$$\eta = O\left(\frac{n^{-5}\tau^{-2R}\log^3(n)}{\log^3(\log(n))}\right)$$
(77)

$$\epsilon = O\left(\frac{n^{-16}\tau^{-6R}\log^4(n)}{\log^4(\log(n))}\right) \tag{78}$$

$$\Delta = O\left(\frac{\log^2(\log(n))}{n^6 \tau^{2R} \log^2(n)}\right). \tag{79}$$

However, recall that in order to maintain the link to PBQC we can only evolve the system for time $\frac{1}{4}Cn\tau^R$, so in this set-up we can only perform a unitary with "computation budget" at most $\|H_{\text{bulk}}\|_{t=1}^{t=1} e^{-13} \tau^{-4R}$. From Lemma 6 the error in the state at the end of the simulation would be:

$$\|e^{-iH_{\text{sim}}t}\rho'e^{iH_{\text{sim}}t} - e^{-i\mathcal{E}(H_{\text{target}})t}\rho'e^{i\mathcal{E}(H_{\text{target}})t}\|_{1}$$

$$\leq O\left(\frac{n^{-15}\tau^{-5R}\log^{4}(n)}{\log^{4}(\log(n))} + \frac{n^{-5}\tau^{-2R}\log^{3}(n)}{\log^{3}(\log(n))}\right).$$
(80)

As in the previous section the ϵ error is small with respect to the computation budget (and can be made arbitrarily smaller by reducing H_{target}), however we cannot achieve a error in η which is small with respect to the computation budget without increasing J. While the η error does not accumulate with time it nevertheless dominates the error for the small computation budget we are considering here, and this error swamps the simulation.

Appendix C Explicit perturbative construction of an attack on PBQC

In this section we investigate the limits on the computational budget for the local unitary in the centre of the bulk, if perturbative simulation techniques are used to create an approximate boundary Hamiltonian that can implement the bulk computation non-locally.

Using perturbative simulations gives worse bounds than the non-perturbative techniques described above, particularly in the case of sparse Hamiltonians. However the perturbative techniques are not optimised for the cases where we are simulating Hamiltonians that have large locality but are sparse. It could be expected that perturbative simulations would perform worse since previous perturbative simulations generically require $\max_i \|h_i\| = O\left(\|H_{\text{target}}\|\text{poly}\left(\frac{1}{\epsilon^k}\right)\right)$ to simulate a k-local H_{target} with a 2-local $H = \sum_i h_i$ while keeping the error and the number of spins fixed [Cao+17; Bra+08; CN18]. In the following section we give an explicit recipe for a perturbative simulation of the boundary Hamiltonian. The interaction strengths of the simulator Hamiltonian is improved over the recipe followed in [KC19; AKC21] by varying the 'heavy' Hamiltonian norm 13.

We want to simulate a n-local bulk Hamiltonian term acting on the central bulk tensor (which generates the general n qubit unitary). This has Pauli rank at most 4^n . The tensor network mapping gives a boundary Hamiltonian, H_{target} , that is a perfect simulation of this bulk operator. The norm and Pauli rank are preserved since the mapping is isometric and stabilizer, however, it is now $O(n\tau^R)$ -local. The initial target Hamiltonian on the boundary before any simulation is therefore,

$$H_{\text{target}} = bP_{O(n\tau^R)},\tag{81}$$

where b is a placeholder for the norm of the bulk term which we will later examine.

To recover a causal boundary Hamiltonian we construct an approximate simulation to H_{target} with reasonable interaction strengths that is 2-local. This section uses perturbative simulation techniques originating in complexity theory. Reducing the locality employs the subdivision gadget Section C.1.1. Simulating a $n\tau^R$ -local Hamiltonian with a 2-local simulator requires $O(R\log(n))$ recursive applications of the subdivision gadget followed by the 3-to-2 gadget.

Since the initial interaction had Pauli rank 4^n , this many recursive simulations are done in parallel to break down the full initial operator. Hence the entire process introduces $O(4^n n \tau^R)$ ancilla qubits. Once the locality is reduced there are additional gadgets to make the boundary Hamiltonian geometrically local, see proof of Theorem 6.10 from [KC19]. However, reducing the locality (to a 2-local but not geometrically local Hamiltonian) limits the computational budget to doubly exponential in R and exponential in n.

C.1 Perturbative simulation tools

Here for completeness we quote some relevant technical results concerning Hamiltonian simulation from the literature.

¹³Perturbative simulations consist of a 'heavy' Hamiltonian and a perturbation. When projected into the low energy subspace the heavy Hamiltonian ensures that the ancillary qubits are in a low energy state that with the perturbation facilitates the more complex interaction being simulated.

Lemma 16 (Second order simulation [BH14]). Let $V = H_1 + \Delta^{\frac{1}{2}}H_2$ be a perturbation acting on the same space as H_0 such that $\max(||H_1||, ||H_2||) \leq \Lambda$; H_1 is block diagonal with respect to the split $\mathcal{H} = \mathcal{H}_- \oplus \mathcal{H}_+$ and $(H_2)_{--} = 0$. Suppose there exists an isometry W such that $Im(W) = \mathcal{H}_-$ and:

$$||WH_{target}W^{\dagger} - (H_1)_{--} + (H_2)_{-+}H_0^{-1}(H_2)_{+-}||_{\infty} \le \frac{\epsilon}{2}$$
(82)

Then $\tilde{H} = H + V\left(\frac{\Delta}{2}, \eta, \epsilon\right)$ simulates H_{target} , provided that $\Delta \geq O\left(\frac{\Lambda^6}{\epsilon^2} + \frac{\Lambda^2}{\eta^2}\right)$.

Lemma 17 (Concatenation of approximate simulation [CMP19]). Let A, B, C be Hamiltonians such that A is a $(\Delta_A, \eta_A, \epsilon_A)$ -simulation of B and B is a $(\Delta_B, \eta_B, \epsilon_B)$ - simulation of C. Suppose $\epsilon_A, \epsilon_B \leq \|C\|$ and $\Delta_B \geq \|C\| + 2\epsilon_A + \epsilon_B$. Then A is a (Δ, η, ϵ) -simulation of C where $\Delta \geq \Delta_B - \epsilon_A$ and

$$\eta = \eta_A + \eta_B + O\left(\frac{\epsilon_A}{\Delta_B - \|C\| + \epsilon_B}\right) \quad and \quad \epsilon = \epsilon_A + \epsilon_B + O\left(\frac{\epsilon_A \|C\|}{\Delta_B - \|C\| + \epsilon_B}\right).$$
(83)

In Section C.2 we use the following technical result.

Lemma 18 (Closed form of δ_x). And element in the series δ defined recursively,

$$\delta_x = \begin{cases} \delta_0 & x = 0\\ 4\sum_{l=0}^{x-1} \frac{\delta_l}{2^{x-l}} & x > 0, \end{cases}$$
 (84)

has the closed form for x > 0,

$$\delta_x = \frac{5^{x-1}}{2^{x-2}} \delta_0. \tag{85}$$

Proof. The first few elements of the series read,

$$\delta_1 = 4 \left\lceil \frac{1}{2} \right\rceil \delta_0 \tag{86}$$

$$\delta_2 = 4 \left[\frac{1}{2^2} + \frac{4}{2^2} \right] \delta_0 \tag{87}$$

$$\delta_3 = 4 \left[\frac{1}{2^3} + \frac{2 \times 4}{2^3} + \frac{4^2}{2^3} \right] \delta_0 \tag{88}$$

$$\delta_4 = 4 \left[\frac{1}{2^4} + \frac{3 \times 4}{2^4} + \frac{3 \times 4^2}{2^4} + \frac{4^3}{2^4} \right] \delta_0 \tag{89}$$

$$\delta_5 = 4 \left[\frac{1}{2^5} + \frac{4 \times 4}{2^5} + \frac{6 \times 4^2}{2^5} + \frac{4 \times 4^3}{2^5} + \frac{4^4}{2^5} \right] \delta_0. \tag{90}$$

We notice the pattern,

$$\delta_x = \frac{2^2}{2^x} \sum_{k=0}^{x-1} {x-1 \choose k} 4^k. \tag{91}$$

We then use the identity $\sum_{k=0}^{m} {m \choose k} 4^k = 5^m$ to obtain the quoted result.

C.1.1 Subdivision gadget used in the construction

The subdivision gadget is used to simulate a k-local interaction by interactions which are at most $\left\lceil \frac{k}{2} \right\rceil + 1$ -local. We want to simulate the Hamiltonian:

$$H_{\text{target}} = \delta_0 (P_A \otimes P_B + P_A^{\dagger} \otimes P_B^{\dagger}) \tag{92}$$

Let $\tilde{H} = H + V$ where:

$$H = \Delta \Pi_{+} \tag{93}$$

$$V = H_1 + \Delta^{\frac{1}{2}} H_2 \tag{94}$$

where:

$$\Pi_{+} = |1\rangle \langle 1|_{w} + |2\rangle \langle 2|_{w} + \dots + |p-1\rangle \langle p-1|_{w}$$

$$\tag{95}$$

$$H_1 = 2\delta_0 \mathbb{1} \tag{96}$$

$$H_2 = \sqrt{\frac{\delta_0}{2}} \left(-P_A \otimes X_w - P_A^{\dagger} \otimes X_w^{\dagger} + P_B \otimes X_w^{\dagger} + P_B^{\dagger} \otimes X_w \right) \tag{97}$$

The degenerate ground space of H has the mediator qubit w in the state $|0\rangle\langle 0|$ so $\Pi_{-}=|0\rangle\langle 0|_{w}$. This gives:

$$(H_1)_{--} = 2\delta_0 \mathbb{1} \otimes |0\rangle \langle 0|_w \tag{98}$$

and:

$$(H_2)_{-+} = \sqrt{\frac{\delta_0}{2}} \left(-P_A \otimes |0\rangle \langle p - 1|_w - P_A^{\dagger} \otimes |0\rangle \langle 1|_w + P_B \otimes |0\rangle \langle 1|_w + P_B^{\dagger} \otimes |0\rangle \langle p - 1|_w \right)$$
(99)

Therefore:

$$(H_2)_{-+}H_0^{-1}(H_2)_{+-} = \delta_0 \left(P_A \otimes P_B + P_A^{\dagger} \otimes P_B^{\dagger} - 2\mathbb{1} \right) \otimes |0\rangle \langle 0|_w$$
 (100)

If we define an isometry W by $W |\psi\rangle_A = |\psi\rangle_A |0\rangle_w$ then:

$$||WH_{\text{target}}W^{\dagger} - (H_1)_{--} + (H_2)_{-+}H_0^{-1}(H_2)_{+-}|| = 0$$
(101)

Therefore Eq. (82) is satisfied for all $\epsilon \geq 0$. So, provided a Δ is picked which satisfies the conditions of Eq. (82), \tilde{H} is a $(\frac{\Delta}{2}, \eta, \epsilon)$ -simulation of H_{target} .

C.2 Limited computational budget with perturbative simulation

At round r we use a "heavy" Hamiltonian of strength,

$$\Delta_r = b\gamma_r^{-2},\tag{102}$$

where γ_r is initially general and we just write the above for algebraic convenience that will become apparent.

Using second order (ϵ, η, Δ) -simulation the errors (Lemma 16) in each round is given by,

$$\epsilon_r \ge O\left(\frac{\Lambda_r^3}{\sqrt{\Delta_r}}\right), \qquad \eta_r \ge O\left(\frac{\Lambda_r}{\sqrt{\Delta_r}}\right)$$
(103)

where $\Lambda = \max\{\left\|H_1^{(r)}\right\|, \left\|H_2^{(r)}\right\|\}.$

We will denote by $h_t^{(r)}$ the norm of the Hamiltonian of the target Hamiltonian that is simulated in round r, and assume b < 1 so that $\sqrt{b} > b$. After enumerating a few rounds of the subdivision gadget (Section C.1.1) the general scaling of the simulation error, ϵ_r , and the Hamiltonian norm as the subdivision is applied recursively is found to be

$$h_t^{(r)} = O\left(b\gamma_r^{-1}\gamma_{r-1}^{-1/2}...\gamma_0^{-1/2^r}\right),\tag{104}$$

$$\epsilon_r \ge O\left(b \frac{\gamma_r}{\left(\gamma_0^{1/2^r} \dots \gamma_{r-1}^{1/2}\right)^3}\right),\tag{105}$$

$$\eta_r \ge O\left(\frac{\gamma_r}{\gamma_{r-1}^{1/2^2} \gamma_{r-2}^{1/2^3} \dots \gamma_0^{1/2^{r+1}}}\right),\tag{106}$$

for r > 1. The convenience of working with γ_r rather that Δ_r becomes apparent since the error and the Hamiltonian are always proportional to b.

Now to turn the products into sums define δ_r by,

$$\gamma_r^{-2} = \tau^{\delta_r \log(n)R},\tag{107}$$

so that now Eq. (104) and Eq. (105) read as:

$$h_t^{(r+1)} = O\left(b\tau^{R\log(n)\sum_{l=0}^r \frac{\delta_l}{2^{r-l}}}\right)$$
 (108)

$$\epsilon_r \ge O\left(b\tau^{-\frac{R\log(n)}{2}\left(\delta_r - 3\sum_{l=0}^{r-1} \frac{\delta_l}{2^{r-l}}\right)}\right)$$
(109)

$$\eta_r \ge O\left(\tau^{-\frac{R\log(n)}{2}}\left(\delta_r - \frac{1}{4}\sum_{l=0}^{\infty} \frac{\delta_l}{2^{r-l}}\right)\right)$$
(110)

We can now analyse what we require to have a good simulation.

From Lemma 17 (if the conditions hold) the final error in the Hamiltonian is given by,

$$\epsilon = \sum_{r=0}^{\log(n)R} \epsilon_r, \qquad \eta = \sum_{r=0}^{\log(n)R} \eta_r. \tag{111}$$

For error in the simulation to be small with respect to the target Hamiltonian norm b, we require,

$$\delta_r > 3\sum_{l=0}^{r-1} \frac{\delta_l}{2^{r-l}}.\tag{112}$$

To ensure this we set $\delta_r = (3+a) \sum_{l=0}^{r-1} \frac{\delta_l}{2^{r-l}}$ for some constant a. This choice also ensures that the conditions in Lemma 17 are satisfied and we The choice of a does not affect the scaling so we set a=1 since Lemma 18 gives a convenient closed form for δ_r (see Section C.1).

The sum in Eq. (108) is now given by,

$$\sum_{l=0}^{r} \frac{\delta_l}{2^{r-l}} = \frac{\delta_0}{2^r} + \sum_{l=1}^{r} \frac{1}{2^{r-l}} \frac{5^{l-1}}{2^{l-2}} \delta_0$$
(113)

$$=\frac{\delta_0}{2^r} + \frac{\delta_0}{2^{r-2}} \sum_{l=1}^r 5^{l-1} \tag{114}$$

$$= \frac{\delta_0}{2^r} + \delta_0 2^{-r} (5^r - 1) \tag{115}$$

$$= \left(\frac{5}{2}\right)^r \delta_0 \tag{116}$$

Hence,

$$h_t^{(r+1)} = O\left(b\tau^{R\log(n)(5/2)^r\delta_0}\right) \tag{117}$$

$$\epsilon_r \ge O\left(b\tau^{-\frac{R\log(n)}{2}\left(\frac{5}{2}\right)^{r-1}\delta_0}\right)$$
 (118)

$$\eta_r \ge O\left(\tau^{-\frac{R\log(n)}{4}\left(\frac{5}{2}\right)^{r-1}\delta_0}\right) \tag{119}$$

The final approximate simulation has,

$$\epsilon \ge O\left(\log(n)Rb\tau^{-R\log(n)\delta_0/4}\right)$$
 (120)

$$\eta \ge O\left(\log(n)R\tau^{-\log(n)R\delta_0/2}\right) \tag{121}$$

$$\Delta \ge \Delta_1 - \epsilon' = b\tau^{\delta_0 R \log(n)} - O(\log(n)Rb\tau^{-R\log(n)\delta_0/4}) \tag{122}$$

since the first round of simulation has the largest upper bound of $\epsilon_1 \geq O\left(b\tau^{-R\log(n)\delta_0/4}\right)$ and $\eta_1 \geq O\left(\tau^{-\log(n)R\delta_0/2}\right)$. The final simulating Hamiltonian is norm,

$$||H_{\text{sim}}|| = O(b\tau^{Rn\log(n)(5/2)^R}\delta_0).$$
 (123)

We require two conditions such that the boundary Hamiltonian is an approximate simulation of the central bulk operation that is causal. Firstly, the simulation Hamiltonian must have small interaction strengths so that the Lieb Robinson is constant, i.e. Eq. (123) must be at most O(1) with respect to R. Secondly the simulation approximation must be small with respect to the target Hamiltonian norm, i.e. from Eq. (120), $O(\log(n)R\tau^{-R\log(n)\delta_0/4}) = O(1)$. In order to do this we are free to chose δ_0 .

To achieve a reasonable Lieb-Robinson velocity it would be helpful to make δ_0 scale as $O\left(\frac{e^{-R}}{nR}\right)$, this would obtain O(1) Lieb-Robinson velocities for b=O(1) norm bulk Hamiltonians. However this leads to a simulation error that completely swamps the target Hamiltonian in Eq. (120). Imposing a reasonable simulation error restricts δ_0 to be a small constant independent of R and n. Once δ_0 is set, to achieve a reasonable Lieb-Robinson velocity from $||H_{\text{sim}}||$ the bulk Hamiltonian norm is forced to be doubly exponentially small in R and singularly exponentially small in R and singularly exponentially small in R and the protocol is trivial.

We have argued that with perturbation gadgets we do not expect to be able to do any better than this limited protocol.

Appendix D Lower bound on simulation from causality

Here we consider a simple causality argument to get a lower bound on the strengths of a 2geometrically local Hamiltonian that simulates a n local one. Consider the target Hamiltonian $H = \frac{1}{2}(\mathbb{1}_A \otimes \mathbb{1}_B + X_A \otimes X_B + Y_A \otimes Y_B + Z_A \otimes Z_B)$. While this Hamiltonian is 2-local we consider A and B being n qubits apart so that the Hamiltonian spreads correlations across n qubits almost instantaneously (clearly a feature of n-local systems). Given an initial state $|\psi\rangle_A\otimes|0\rangle_B$ evolution under this Hamiltonian for a time t is given by,

$$e^{-itH} |\psi\rangle_A |0\rangle_B = \cos(t) |\psi\rangle_A |0\rangle_B - i\sin(t) |0\rangle_A |\psi\rangle_B.$$
 (124)

Hence in time $\pi/2$ the information at A has been transferred to B under the Hamiltonian.

If we now simulate this Hamiltonian with $\tilde{H} = \sum_{i=1}^{n-1} \tilde{h}_{i,i+1}$ where $\tilde{h}_{i,i+1} = \frac{\tau}{2} (\mathbb{1}_i \otimes \mathbb{1}_{i+1} + X_i \otimes X_{i+1} + Y_i \otimes Y_{i+1} + Z_i \otimes Z_{i+1})$. Given the initial state $|\psi\rangle_1 |0\rangle_n$, we impose the state after evolution for $t = \pi/2$ must be $|0\rangle_1 |\psi\rangle_n$ to emulate the target Hamiltonian. The interaction strength of the simulator Hamiltonian must be $\tau = n$ in order to propagate the information through the chain of interactions in the same time. Hence this gives an example of a sparse n-local Hamiltonian that a universal geometrically local Hamiltonian will have to simulate which requires interaction strength linear in n. While we give a specific example of a simulating Hamiltonian it is clear that the form of the interactions cannot be modified to propagate information faster since each link is maximally entangling.

Consider an approximation in the time dynamics simulator, $\left\| e^{-i\tilde{H}\pi/2} \left| \psi \right\rangle_1 \left| 0 \right\rangle_n - \left| 0 \right\rangle_n \left| \psi \right\rangle_1 \right\|_1 \le \epsilon$. As in Theorem 14 we may hope to find a lower bound on the interaction strength that encorportates the error in the simulation. For this example we can translate the error in the state to,

$$\left|\cos^n\left(\frac{\tau\pi}{2n}\right)\right|^2 \le \epsilon. \tag{125}$$

We can see here if τ scales sub-linearly with n then for large n we have $\left|\cos^n\left(\frac{\tau\pi}{2n}\right)\right|^2=1$ and the simulator state is orthogonal to the target. So in this case we are unable to obtain an interaction strength bound incorporating more parameters of the simulation.

This investigation, while rudimentary, intuitively demonstrates the lower bounds presented in this paper are not immediate from causality arguments. We leave further investigation into other methods of reasoning about simulation lower bounds to further work.

References

- [MPS19] Alex May, Geoff Penington, and Jonathan Sorce. Holographic scattering requires a connected entanglement wedge. Tech. rep. 2019. arXiv: 1912.05649v3.
- [Pas+15] Fernando Pastawski, Beni Yoshida, Daniel Harlow, and John Preskill. "Holographic quantum error-correcting codes: toy models for the bulk/boundary correspondence". In: Journal of High Energy Physics 2015.6 (June 2015).
- [Hay+16]Patrick Hayden, Sepehr Nezami, Xiao-Liang Qi, Nathaniel Thomas, Michael Walter, and Zhao Yang. "Holographic duality from random tensor networks". In: Journal of High Energy Physics 2016.11 (Nov. 2016).
- [KC19] Tamara Kohler and Toby Cubitt. Toy Models of Holographic Duality between local Hamiltonians. Tech. rep. 2019. arXiv: 1810.08992v3.
- [Koh+20]Tamara Kohler, Stephen Piddock, Johannes Bausch, and Toby Cubitt. Translationally-Invariant Universal Quantum Hamiltonians in 1D. Tech. rep. 2020. arXiv: 2003. 13753v1.
- [AKC21] Harriet Apel, Tamara Kohler, and Toby Cubitt. "Holographic duality between local Hamiltonians from random tensor networks". In: (2021). arXiv: 2105.12067.
- Xiao-Liang Qi and Zhao Yang. Butterfly velocity and bulk causal structure. Tech. rep. [QY17] 2017. arXiv: 1705.01728v1.
- [May19] Alex May. Quantum tasks in holography. Tech. rep. 2019. arXiv: 1902.06845v7.
- [DC22a]Kfir Dolev and Sam Cree. Holography as a resource for non-local quantum computation. 2022. arXiv: 2210.13500 [quant-ph].

- [Buh+14] Harry Buhrman, Nishanth Chandran, Serge Fehr, Ran Gelles, Vipul Goyal, Rafail Ostrovsky, and Christian Schaffner. "Position-Based Quantum Cryptography: Impossibility and Constructions". In: SIAM Journal on Computing 43.1 (2014), pp. 150–178.
- [BK11b] Salman Beigi and Robert König. "Simplified instantaneous non-local quantum computation with applications to position-based cryptography". In: New Journal of Physics 13.9 (2011), p. 093036.
- [CM22] Sam Cree and Alex May. Code-routing: a new attack on position verification. 2022. arXiv: 2202.07812 [quant-ph].
- [DC22b] Kfir Dolev and Sam Cree. Non-local computation of quantum circuits with small light cones. 2022. arXiv: 2203.10106 [quant-ph].
- [Jun+22] Marius Junge, Aleksander M. Kubicki, Carlos Palazuelos, and David Pérez-García. "Geometry of Banach Spaces: A New Route Towards Position Based Cryptography". In: Communications in Mathematical Physics 394.2 (2022), pp. 625–678.
- [May22] Alex May. "Complexity and entanglement in non-local computation and holography". In: Quantum 6 (2022), p. 864.
- [AZ18] Dorit Aharonov and Leo Zhou. "Hamiltonian Sparsification and Gap-Simulation". en. In: (2018).
- [Tom+13] Marco Tomamichel, Serge Fehr, Jędrzej Kaniewski, and Stephanie Wehner. "A Monogamy-of-Entanglement Game With Applications to Device-Independent Quantum Cryptography". In: (2013). arXiv: 1210.4359v3.
- [Spe16] Florian Speelman. "Instantaneous Non-Local Computation of Low T-Depth Quantum Circuits". en. In: (2016).
- [BS23] Valérie Bettaque and Brian Swingle. "NoRA: A Tensor Network Ansatz for Volume-Law Entangled Equilibrium States of Highly Connected Hamiltonians". In: (2023). arXiv: 2303.16946v3.
- [BK11a] Salman Beigi and Robert König. "Simplified instantaneous non-local quantum computation with applications to position-based cryptography". In: (2011). arXiv: 1101. 1065v3.
- [Dol] Kfir Dolev. "Constraining the doability of relativistic quantum tasks". In: (). arXiv: 1909.05403v1.
- [CMP19] Toby Cubitt, Ashley Montanaro, and Stephen Piddock. *Universal quantum Hamiltonians*. 2019.
- [Cao+17] Yudong Cao, Sabre Kais, Barbara Terhal, and Richard Jozsa. "Efficient optimization of perturbative gadgets". In: 17 (9 2017), pp. 779–0809.
- [Bra+08] Sergey Bravyi, David P Divincenzo, Daniel Loss, and Barbara M Terhal. "Simulation of Many-Body Hamiltonians using Perturbation Theory with Bounded-Strength Interactions". In: (2008).
- [CN18] Yudong Cao and Daniel Nagaj. "Perturbative gadgets without strong interactions". In: (2018).
- [Mas23] Lluis Masanes. "Discrete holography in dual-unitary circuits". In: arXiv:2301.02825 (2023).
- [Har+23] Dylan Harley, Ishaun Datta, Frederik Ravn Klausen, Andreas Bluhm, Daniel Stilck França, Albert Werner, and Matthias Christandl. "Going Beyond Gadgets: The Importance of Scalability for Analogue Quantum Simulators". In: arXiv: 2306.13739 (2023).
- [BCK15] Dominic W. Berry, Andrew M. Childs, and Robin Kothari. "Hamiltonian Simulation with Nearly Optimal Dependence on all Parameters". In: 2015 IEEE 56th Annual Symposium on Foundations of Computer Science. 2015, pp. 792–809.
- [BH14] Sergey Bravyi and Matthew Hastings. On complexity of the quantum Ising model. 2014.